



Strange messenger: A new history of hydrogen on Earth, as told by Xenon

Kevin J. Zahnle^{a,*}, Marko Gacesa^b, David C. Catling^c

^aSpace Science Division, NASA Ames Research Center, MS 245-3, Moffett Field, CA 94035, USA

^bSpace Sciences Lab, UC Berkeley, CA 94720, USA

^cDepartment of Geology, University of Washington, Seattle, WA, USA

Received 24 May 2018; accepted in revised form 15 September 2018; Available online 6 October 2018

Abstract

Atmospheric xenon is strongly mass fractionated, the result of a process that apparently continued through the Archean and perhaps beyond. Previous models that explain Xe fractionation by hydrodynamic hydrogen escape cannot gracefully explain how Xe escaped when Ar and Kr did not, nor allow Xe to escape in the Archean. Here we show that Xe is the only noble gas that can escape as an ion in a photo-ionized hydrogen wind, possible in the absence of a geomagnetic field or along polar magnetic field lines that open into interplanetary space. To quantify the hypothesis we construct new 1-D models of hydrodynamic diffusion-limited hydrogen escape from highly-irradiated CO₂-H₂-H atmospheres. The models reveal three minimum requirements for Xe escape: solar EUV irradiation needs to exceed 10× that of the modern Sun; the total hydrogen mixing ratio in the atmosphere needs to exceed 1% (equiv. to 0.5% CH₄); and transport amongst the ions in the lower ionosphere needs to lift the Xe ions to the base of the outflowing hydrogen corona. The long duration of Xe escape implies that, if a constant process, Earth lost the hydrogen from at least one ocean of water, roughly evenly split between the Hadean and the Archean. However, to account for both Xe's fractionation and also its depletion with respect to Kr and primordial ²⁴⁴Pu, Xe escape must have been limited to small apertures or short episodes, which suggests that Xe escape was restricted to polar windows by a geomagnetic field, or dominated by outbursts of high solar activity, or limited to transient episodes of abundant hydrogen, or a combination of these. Xenon escape stopped when the hydrogen (or methane) mixing ratio became too small, or EUV radiation from the aging Sun became too weak, or charge exchange between Xe⁺ and O₂ rendered Xe neutral. In our model, Xe fractionation attests to an extended history of hydrogen escape and Earth oxidation preceding and ending with the Great Oxidation Event (GOE). Published by Elsevier Ltd. This is an open access article under the CC BY-NC-ND license (<http://creativecommons.org/licenses/by-nc-nd/4.0/>).

Keywords: Earth atmospheric evolution; Noble gases; Great oxidation event

1. INTRODUCTION

Hydrogen escape offers a plausible explanation for the oxygenation of Earth's atmosphere (Catling et al., 2001; Zahnle et al., 2013). The mechanism is straightforward: hydrogen escape irreversibly oxidizes the Earth, beginning with the atmosphere, and then working its way down. The

importance of hydrogen in Earth's early atmosphere in promoting the formation of molecules suitable to the origin of life was recognized before the dawn of the space age (Urey, 1952). The subsequent importance of hydrogen escape in promoting chemical evolution in a direction suitable to creating life was also recognized by Urey (1952). The potential importance of hydrogen escape in driving biological evolution toward oxygen-using aerobic ecologies has not been as fully appreciated, but it is quite clear that the bias is there.

The hydrogen that escapes derives mostly from water. It can be liberated from water by photolysis, by photosynthe-

* Corresponding author.

E-mail address: Kevin.J.Zahnle@NASA.gov (K.J. Zahnle).

sis followed by fermentation or diagenesis of organic matter releasing H_2 or CH_4 , or by oxidation of the crust and mantle. A smaller source was the hydrogen in hydrocarbons delivered by asteroids and comets. Earth's tiny Ne/N ratio, two elements that are equally abundant in the Sun, argues persuasively against a significant primary reservoir of gravitationally-captured solar nebular gases (Aston, 1924; Brown, 1949; Zahnle et al., 2010). Hydrogen is common to many atmospheric gases, but above Earth's water vapor cold trap only H_2 or CH_4 can be abundant. At still higher altitudes, atmospheric photochemistry decomposes CH_4 into H_2 and other products; thus, even if CH_4 were more abundant near the surface, H_2 would be the more abundant species at the top of the atmosphere.

Neither hydrogen nor methane leave much of a signal in the geologic record. The D/H ratio in old rocks has been interpreted as suggesting considerable hydrogen escape early in Earth's history (Pope et al., 2012), but the argument does not appear to have been widely accepted (e.g., Korenaga et al., 2017), because the D/H ratio is relatively susceptible to alteration under diagenesis. In the late Archean ca 2.6–2.8 Ga there is circumstantial evidence that biogenic methane was present in the atmosphere, implicated in the generation of isotopically light carbon (Hayes, 1994; Hinrichs, 2002; Zerkle et al., 2012), and in the generation of “mass-independent” isotopic fractionations of sulfur (“MIF-S”, Zahnle et al., 2006).

Here we discuss new evidence from a strange messenger that suggests that Earth's atmosphere, for much of the first half of its history, contained a great deal of hydrogen or methane, and that the amount of hydrogen escape may have been much greater than has been appreciated.

1.1. Xenon's story

Xenon is the heaviest gas found in natural planetary atmospheres. It would therefore seem the least likely to escape to space. Yet there is more circumstantial evidence that xenon has escaped from Earth than for any element other than helium.

The evidence is of three kinds. First, the nine stable isotopes of atmospheric xenon are strongly mass fractionated compared to any known solar system source. The magnitude of the fractionation – about 4% per amu, or 60% from ^{124}Xe to ^{136}Xe – is very great. The fractionation is easily seen in Fig. 1, which compares Xe to Kr in a variety of solar system materials.

Second, atmospheric Xe is depleted with respect to meteorites by a factor of 4–20 when compared to krypton. The elemental depletion is also obvious in Fig. 1. Xenon's low abundance relative to krypton, when compared to carbonaceous chondrites, has been called the “missing xenon” problem (Ozima and Podosek, 1983).

Third, xenon's radiogenic isotopes are much less abundant than they should be when measured against the presumed cosmic abundances of two extinct parents. The disappearance of radiogenic Xe does not demand fractionating xenon escape; it can be accommodated by a wide range of speculative escape mechanisms, such as giant impacts, but it does set some limits.

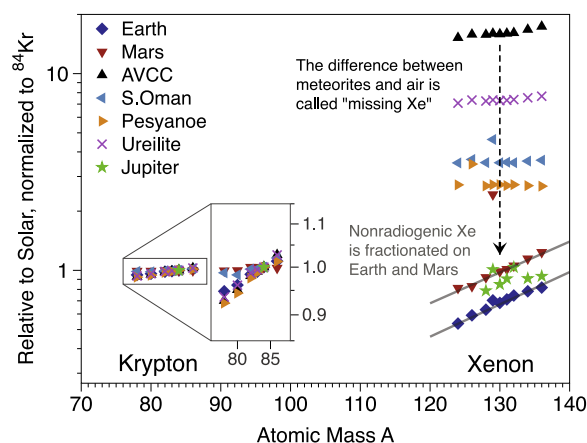


Fig. 1. Xenon and krypton isotopes of Earth (air), Mars (atmosphere), average carbonaceous chondritic meteorites (AVCC), a gas-rich enstatite chondrite (S. Oman), a gas-rich enstatite achondrite (Pesyanoe), a ureilite (Havero), and Jupiter, all normalized against solar abundances and plotted on a scale where ^{84}Kr is one. Meteorite data are from Pepin (1991), Mars from SNC meteorites (Swindle and Jones, 1997) and Jupiter from the Galileo Probe (Atreya et al., 2003). Solar isotopes are from Meshik et al. (2014). The straightforward interpretation of Xe's depletion and mass fractionation is that Xe has preferentially escaped from the atmospheres of Earth and Mars. The inset shows Kr isotopes, the striking features of which are the kinship between Mars and solar on one hand, and the kinship between Earth and meteorites on the other. The modest fractionations seen in Kr all fall within the range of known meteoritic sources and hence cannot be attributed unambiguously to escape.

No more than 7% of the ^{129}Xe in Earth's atmosphere derives from decay of ^{129}I (15.7 Myr half life) (Pepin, 2006). This is only 1% of what Earth could have, given the estimated abundance of iodine in the Earth and the inferred primordial relative abundance of ^{129}I in meteorites (Tolstikhin et al., 2014). Moreover, some or much of the excess ^{129}Xe could be cometary (Marty et al., 2017). Clearly xenon escape was pervasive early in the history of Earth or the materials it was made from. However, because ^{129}Xe escape may not be pertinent to Xe fractionation, we will not make use of the ^{129}I – ^{129}Xe system in this study.

A more useful constraint comes from spontaneous fission of ^{244}Pu (half life 80 Myr), which spawns a distinctive spectrum of heavy xenon isotopes. The initial abundance of ^{244}Pu in Earth can be estimated from Earth's U abundance and the Pu/U ratio in meteorites. The amount of fissionogenic Xe in the atmosphere is determined from the difference between a smooth mass fractionation process acting on Earth's primordial Xe (U-Xe) and what is actually in the atmosphere (Pepin, 2000, 2006). It turns out that only about 20% of the expected amount of fissionogenic Xe is in the atmosphere, and there is much less in the mantle (Tolstikhin et al., 2014). Retention of 20% of fissionogenic Xe sets a bound on Xe escape taking place after plutonium's daughters were degassed.

Spontaneous fission of ^{238}U (half life 4.47 Gyr) has generated about 5% as much fissionogenic Xe as Pu. It is seen in mantle samples, but taking into account that most Xe from ^{238}U must still be in the mantle, it cannot be responsible for

more than $\sim 10\%$ of the fissiogenic Xe in the atmosphere, which is small compared to the other uncertainties.

Until recently, despite the hint from ^{244}Pu that not all Xe loss was early, it had generally been supposed that xenon was fractionated and lost through an energetic process unique to the early solar system, probably hydrodynamic hydrogen escape powered by copious EUV (“extreme ultraviolet radiation”) emitted by the active young Sun (Sekiya et al., 1980; Hunten et al., 1987; Sasaki and Nakazawa, 1988; Pepin, 1991, 2006; Tolstikhin and O’Nions, 1994; Dauphas, 2003; Dauphas and Morbidelli, 2014). Vigorous hydrodynamic hydrogen escape can be an effective way to mass fractionate heavy gases (Sekiya et al., 1980; Zahnle and Kasting, 1986; Hunten et al., 1987; Sasaki and Nakazawa, 1988; Pepin, 1991; Dauphas and Morbidelli, 2014). Heavy atoms escape because collisions with the out-bound hydrogen push them outwards faster than gravity can pull them back. Because lighter atoms escape preferentially, the rump atmosphere becomes enriched in heavier atoms and isotopes. As Xe is the heaviest gas, all the other gases must also escape. But with the possible exception of neon (Sasaki and Nakazawa, 1988), the other gases display no isotopic evidence of having done so. Workarounds have been to propose that Kr and the other noble gases escaped quantitatively during the hydrodynamic escape episode, while leaving some fractionated Xe behind. The lighter noble gases would later be resupplied by a process that did not supply much xenon; several different processes have been suggested (Sasaki and Nakazawa, 1988; Pepin, 1991; Tolstikhin and O’Nions, 1994; Dauphas, 2003; Dauphas and Morbidelli, 2014). The discovery that atmospheric Kr is isotopically lighter than the Kr found in the mantle (Holland et al., 2009) appears to contradict models that resupply the atmosphere by degassing the mantle but fits well with models that resupply the atmosphere with (hypothetical) Xe-depleted comets (Dauphas and Morbidelli, 2014).

A feature common to all previous hydrodynamic escape models is that hydrogen escape fluxes large enough to power Xe escape would have been limited to Earth’s first ~ 100 Myrs when the young Sun was still an enormous EUV source (Pepin, 2013). New evidence now indicates that xenon’s mass fractionation evolved over the first half of Earth’s history, only converging with modern air between 1.8 Ga and 2.5 Ga (Pujol et al., 2011, 2013; Avice et al., 2018; Warr et al., 2018). The new evidence comes from the isotopic compositions of trapped atmospheric xenon recovered from several ancient (2–3.5 Ga) rocks (Srinivasan, 1976; Pujol et al., 2009, 2011, 2013; Holland et al., 2013; Avice et al., 2018; Bekaert et al., 2018). The recovered samples of Archean xenon resemble modern air, but they are less strongly mass fractionated. We show some examples in Fig. 2. The full suite of data compiled by Avice et al. (2018) are plotted in summary form in Fig. 3, where we have compared xenon’s story to oxygen’s and sulfur’s.

The evidence that Xe alone escaped among the noble gases requires a mechanism unique to Xe. The evidence that Xe escape continued through the Archean requires a mechanism that can work in Earth’s Archean atmosphere, and

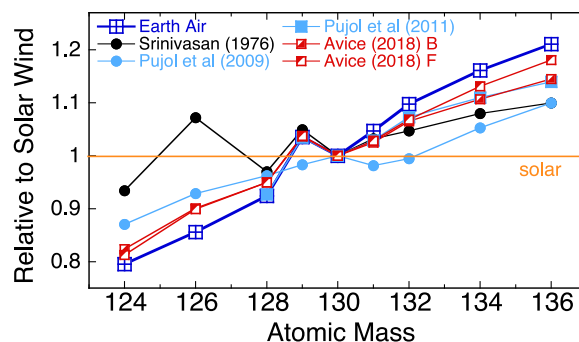


Fig. 2. Xenon trapped in Archean rocks (Srinivasan, 1976; Pujol et al., 2009; Pujol et al., 2011; Avice et al., 2018) is less fractionated than Xe in modern air. Isotopic abundances are each normalized to solar (Meshik et al., 2014), and Xe^{130} is normalized to one. “Avice (2018) B” refers to a Barberton quartz dated to 3.2 ± 0.1 Ga. “Avice (2018) F” refers to a Fortescue quartz with an assigned age of 2.7 Ga. Evidently Xe was escaping from Earth during the Archean.

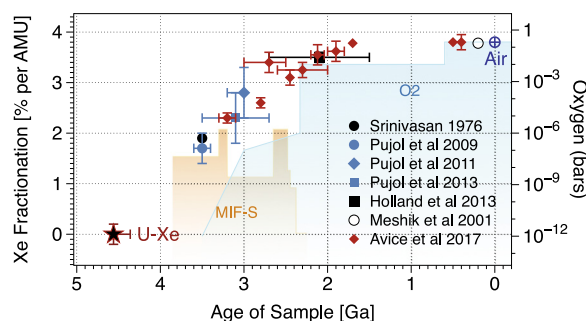


Fig. 3. The history of xenon mass fractionation on Earth compared to schematic histories of mass-independent fractionation of sulfur (S-MIF, orange) and to the inferred history of oxygen (O_2 , blue) in air. Earth’s original isotopic structure is labeled “U-Xe,” a kind of primordial Xe that is like solar Xe but depleted in Xe’s two heaviest isotopes (Pepin, 2006). Adapted from Avice et al. (2018). (For interpretation of the references to color in this figure legend, the reader is referred to the web version of this article.)

therefore one that can work at more modest levels of solar EUV. Hydrodynamic xenon escape as an ion is such a mechanism. It retains the advantages of traditional hydrodynamic escape without the two disadvantages of requiring too much solar EUV energy and predicting even greater amounts Kr and Ar fractionation. In particular, the fractionation mechanism is the same – collisions push ions outwards, and gravity pulls them back – as in neutral hydrodynamic escape. The difference is that the collisional cross sections are much bigger between ions.

What makes it possible for Xe alone of the noble gases to escape as an ion in hydrogen is that Xe is the only noble gas more easily ionized than hydrogen (Table 1). Hydrogen will be partially photo-ionized. In a hydrogen-dominated hydrodynamic wind, gases that are more difficult to ionize than hydrogen will tend to be present as neutrals. But Xe, being more easily ionized than H or H_2 , will tend to be present as an ion. First, Xe can be photo-ionized by UV radiation ($91.2 < \lambda < 102.3$ nm) to which H and H_2 are

Table 1
Some interesting ionization thresholds (NIST).

	I_p [eV]	λ [nm]		I_p [eV]	λ [nm]		I_p [eV]	λ [nm]
Ar	15.76	78.67	CO ₂	13.78	89.98	CH ₄	12.61	98.33
N ₂	15.58	79.59	O	13.62	91.04	Xe	12.13	102.2
H ₂	15.43	80.36	H	13.60	91.17	O ₂	12.07	102.7
N	14.53	85.34	HCN	13.60	91.17	C ₂ H ₂	11.40	108.8
CO	14.01	88.48	OH	13.02	95.24	NO	9.26	133.9
Kr	14.00	88.57	H ₂ O	12.62	98.26	HCO	8.12	152.7

transparent. Second, as we shall show, Xe can be ionized by charge exchange with H⁺. Third, Xe⁺ can be slow to recombine in hydrogen. In particular, the important reaction Kr⁺ + H₂ → KrH⁺ + H is fast. The KrH⁺ ion quickly dissociatively recombines: KrH⁺ + e⁻ → Kr + H. The corresponding reaction Xe⁺ + H₂ does not occur (Anicich, 1993). Thus Xe⁺ tends to persist in H₂ whereas Kr⁺ is quickly neutralized.

Ions interact strongly with each other through the Coulomb force, especially at low temperatures. If the escaping hydrogen is significantly ionized, and if the ions are also escaping, the strong Coulomb interactions between ions permit Xe⁺ to escape at hydrogen escape fluxes well below what would be required for neutral Kr or even neutral Ne to escape. Under these circumstances fractionating hydrodynamic escape can apply uniquely to Xe among the noble gases over a wide range of hydrogen escape fluxes, despite Xe's greater mass.

Parenthetically, it has been speculated that trapping Xe⁺ in organic hazes on Archean Earth could lead to a way to fractionate Xe in the atmosphere (Hébrard and Marty, 2014; Avicé et al., 2018). Indeed, it has recently been shown that isotopically ancient Xe was trapped, and has remained trapped, in ancient organic matter on Earth (Bekaert et al., 2018). Ionized Xe can be chemically incorporated into organic material (Frick et al., 1979; Marrocchi et al., 2011; Marrocchi and Marty, 2013). The trapped Xe is mass fractionated with a ~ 1% per amu preference for the heavier isotopes (Frick et al., 1979; Marrocchi et al., 2011; Marrocchi and Marty, 2013). For trapping to work as a fractionating mechanism, most of Earth's Xe must have resided in organic matter through much of the Hadean and Archean, and the process must have run through several rock weathering cycles to build up the fractionation, yet there still needs to be a Xe-specific escape process, as otherwise when the trapped Xe is released by weathering the atmosphere would regain its original unfractionated isotopic composition. We think it simpler to assign both depletion and fractionation to the hydrodynamic escape process, so we have not pursued this more complicated scenario here.

Martian atmospheric Xe as determined from SNC meteorites (Swindle and Jones, 1997) superficially resembles Xe in Earth's air, which makes it tempting to imagine that Earth and Mars received their Xe from a common fractionated source. However, martian Xe has been less impacted by escape. Martian Xe is 50% less depleted than Earth's (well-seen in Fig. 1) and it has been fractionated by about 2.5% per amu from what was initially solar Xe, whilst Earth's was fractionated by about 4% per amu from

U-Xe. Moreover, Xe fractionation on Mars took place very early (Cassata, 2017). These differences imply parallel evolution rather than a common source.

To assess Xe⁺ escape from Earth's ancient atmosphere, we first need to develop a model of irradiation-fueled diffusion-limited hydrodynamic hydrogen escape that includes a full energy budget and that computes temperature and ionization as well as the escape flux. This project is described in detail in Appendix A. A subset of results pertinent to Xe escape are summarized in Section 2. Section 3 addresses Xe chemistry and Xe escape, although the details of the model are relegated to Appendix B, as the notation and development follow directly from the hydrogen escape model developed in Appendix A. Section 4 addresses histories of atmospheric hydrogen and hydrogen escape that best reproduce the observed history of Xe fractionation and depletion. Section 5 recapitulates the chief results and chief caveats, and suggests directions for further research. Appendix C provides a complete alphabetized table of symbols used in the text and Appendices.

2. HYDROGEN ESCAPE FROM A CO₂-RICH ATMOSPHERE

The general problem of irradiation-driven thermal escape from planetary atmosphere can get very complicated. Here we wish to develop a description of hydrogen escape in the presence of a static background atmosphere suitable for investigating Xe escape. The heavy gases in Earth's Archean atmosphere were likely N₂ and CO₂. We simplify the problem by considering a CO₂-H₂ atmosphere. We chose CO₂ rather than N₂ because we wished to consider a case in which both radiative heating and radiative cooling are important to the energy budget (Kulikov et al., 2007). We will argue that, to first approximation, photochemistry in the CO₂-H₂ atmosphere allows CO₂ to persist while H₂ persists. Our minimum system therefore comprises only H, H₂ and CO₂ as neutral species. We include 5 ions: H⁺, H₂⁺, H₃⁺, CO₂⁺, and HCO⁺. We assume local photochemical equilibrium for the ions, which is a good approximation for the molecular ions, less good for H⁺ at high altitudes. This minimal system omits N₂, N, CO, O, O₂, NO, and their ions. The chemistry is fully described and summarized in Table A.2 in Appendix A.

2.1. Radiation

The two essential free parameters in irradiation-driven thermal hydrogen escape are solar irradiation S and the hydrogen mixing ratio f_{H_2} . Hydrogen efficiently absorbs

radiation at wavelengths $\lambda < 91.2$ nm. This serves as a practical definition of EUV. Water vapor and CO₂ absorb efficiently at wavelengths shorter than $\lambda < 200$ nm. This is a useful definition of far ultraviolet radiation (FUV). The EUV is often lumped together with X-rays as XUV, a convenience that exploits the relative availability of stellar X-ray luminosities.

It is observed that older sunlike stars emit less X-ray and FUV radiation (Zahnle and Walker, 1982; Ribas et al., 2005; Claire et al., 2012; Tu et al., 2015). The observations are sparse enough to be fit to power laws of the form $F_{\text{xuv}} \propto t^{-a}$, where t is the age of the star, and the power a is of order unity. A popular parameterization of the average solar F_{xuv} at Earth is

$$F_{\text{xuv}} = 5(4.5/t)^{1.24} \text{ ergs cm}^{-2} \text{ s}^{-1} \quad (1)$$

where t is the age of the Sun in Gyrs (Ribas et al., 2005). At very early times, say $t < 0.1$ Gyr, this saturates to $F_{\text{xuv}} \approx 400 \text{ ergs cm}^{-2} \text{ s}^{-1}$. FUV radiation does not decay as quickly as XUV, but for present purposes we will ignore this detail, and lump the entire XUV and FUV emission together as a single multiple S of the modern Sun,

$$S(t) \equiv F_{\text{xuv}}/F_{\text{xuv}\odot}. \quad (2)$$

Tu et al. (2015) compare several different models; they estimate that $5 < S < 10$ at 3.5 Ga and $10 < S < 40$ at 4.0 Ga, corresponding to $1 < a < 1.7$. This does not take into account the factor five variation in XUV between active and quiet Sun. With variability included, we might expect $2 < S < 20$ at 3.5 Ga and $1 < S < 10$ at 2.5 Ga.

2.2. Vertical structure, method of solution, and the outer boundary conditions

Vertical structure and transport equations are simplified from the self-consistent 5 moment approximation to multi-component hydrodynamic flow presented by Schunk and Nagy (1980). We merge this description with the description of two component diffusion given by Hunten (1973) to express collision terms as binary diffusion coefficients and to include parameterized Eddy diffusivity in the lower atmosphere. We make several other major simplifications: (i) We assume spherical symmetry. (ii) We ignore diurnal cycles and latitudinal differences. (iii) We presume that H and H₂ flow outward at the same velocity u . (iv) As we are considering a relatively dense gas, we use a single temperature T for all species. (v) We presume that CO₂ does not escape, and thus that hydrogen must diffuse through the CO₂. (vi) We neglect thermal conduction, which becomes a relatively small term in the energy budget at the high levels of solar irradiation needed if Xe is to escape. (vii) We neglect the solar wind, collisional ionization by exogenous particles, and energy flows between different regions of the magnetosphere.

The equations and approximations are developed and fully described in Appendix A. The five basic equations to be solved are Eq. (A.37) for the hydrogen velocity $u(r)$; Eqs. (A.39) and (A.40) for the atomic and molecular hydrogen number densities $n_1(r)$ and $n_2(r)$, respectively; Eq. (A.42) for the CO₂ number density $n_3(r)$; and Eq. (A.51)

for the temperature $T(r)$. The system is solved with the shooting method, integrating upward from a lower boundary density $n(r_0) = 1 \times 10^{13} \text{ cm}^{-3}$, which is below the homopause. The total H₂ mixing ratio $f_{\text{H}_2} (= 0.5f_{\text{H}} + f_{\text{H}_2} + 2f_{\text{CH}_4} + \dots)$ and the total hydrogen escape flux $\phi_{\text{H}_2} (= 0.5\phi_{\text{H}} + \phi_{\text{H}_2} + 2\phi_{\text{CH}_4} + \dots)$ at the lower boundary are treated as independent free parameters.

We seek the unique transonic solution that has just enough energy at the critical point to escape, in keeping with the philosophy that nothing that happens beyond the critical point of a transonic wind can influence the atmosphere at the lower boundary. The energy criterion is given by Eq. (A.53). The transonic solution makes the simplifying assumption that conditions far from Earth are ignorable. This assumption is probably very good for calculating the hydrogen escape flux, which is determined by conditions much deeper in the atmosphere where the bulk of XUV radiation is absorbed. Subsonic solutions require additional parameters to describe the conditions of interplanetary space. As a practical matter, differences between the transonic solution and a relevant subsonic solution are negligible save at great distances (Kasting and Pollack, 1983). We solve for the solar irradiation S required to support ϕ_{H_2} by iterating S using bisection.

2.3. Snapshots taken from a particular model for purposes of illustration

It is helpful to illustrate some properties of a particular model. For this purpose we have chosen a model (hereafter referred to as the “nominal” model) that lies well within the field of models in which Xe escape is predicted to take place. The key parameters are a relatively high EUV flux ($S = 20$) and a relatively high hydrogen mixing ratio ($f_{\text{H}_2} = 0.03$). The high S of the nominal model would be typical before 4.0 Ga but rare after 3.5 Ga. Other nominal parameters are a lower boundary density $n(r_0) = 1 \times 10^{13} \text{ cm}^{-3}$, neutral eddy diffusivity $K_{zz} = 2 \times 10^6 \text{ cm}^2 \text{ s}^{-1}$, and spherical symmetry. Our models of hydrogen escape are not very sensitive to these other parameters. The hydrogen escape flux in this particular model is $\phi_{\text{H}_2} = 7.2 \times 10^{11} \text{ cm}^{-2} \text{ s}^{-1}$, equivalent to 82% of the diffusion-limited flux (Eq. (A.44)).

Fig. 4 shows the temperature and the densities of the ions and neutrals as a function of altitude in the nominal model; the two panels differ only on how the altitude axis is scaled. The linear scale effectively illustrates the extent of the hydrogen atmosphere, while hiding everything else. The logarithmic scaling of altitude focuses attention on the structure of the atmosphere, in which a cold CO₂-rich layer supporting a client population of cold molecular ions is overlain by warm hydrogen and atomic ions. Other aspects of the nominal model and other models are discussed in more detail in Appendix A.

2.4. Many solutions

Fig. 5 presents results from a basic parameter survey of CO₂-H₂ atmospheres. The plot shows how the total hydro-

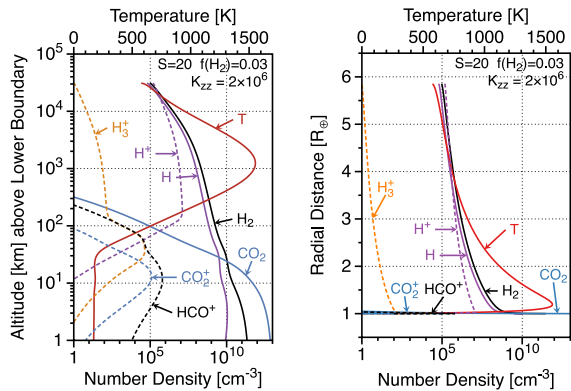


Fig. 4. Temperature and densities of neutrals and ions as a function of altitude in an exemplary model, which we call the “nominal” model ($S = 20$, $f_{\text{H}_2} = 0.03$, and $K_{zz} = 2 \times 10^6 \text{ cm}^2 \text{ s}^{-1}$, for which $\phi_{\text{H}_2} = 7.2 \times 10^{11} \text{ cm}^{-2} \text{ s}^{-1}$.) This nominal model was chosen to illustrate conditions in which Xe^+ escape is expected; the high S of the nominal model would be a rare occurrence later than 3.5 Ga. Altitude is measured from an arbitrary lower boundary where the total density $n(r_0) = 1 \times 10^{13} \text{ cm}^{-3}$. The logarithmic scale best illustrates the overall structure of the upper atmosphere, which features a warm ionized hydrogen exosphere above a cold layer of molecular ions. The linear scale better illustrates the extent of the hydrogen exosphere.

gen escape flux ϕ_{H_2} changes in response to changing solar irradiation S and hydrogen mixing ratios f_{H_2} . Our results (blue circles) in Fig. 5 are compared to two limits often encountered in the literature. The so-called energy-limited flux compares the XUV energy absorbed to the energy required to lift a given mass out of Earth’s potential well and into space (Watson et al., 1981). Details are lumped together in an efficiency factor η that is often taken to lie between 0.1 and 0.6 (Lammer et al., 2013; Bolmont et al., 2017). In one version of the energy limit, all XUV photons that can be directly absorbed by hydrogen ($\lambda < 91.2 \text{ nm}$) contribute to escape. This limit is labeled “Energy-limit (XUV)” in Fig. 5. A second energy limit includes all solar radiation absorbed above a fixed lower boundary. This includes FUV radiation absorbed by CO_2 . This outer limit is labeled “Energy-limit (XUV + FUV)” in Fig. 5. The relevant equations, Eqs. (A.10) and (A.11) in Appendix A, are evaluated with $\eta = 0.5$ to facilitate comparisons with the detailed model. The diffusion-limited flux, the upper bound on how fast hydrogen can diffuse through a hydrostatic atmosphere of CO_2 , is derived in Appendix A in the limit of constant mixing ratios (Zahnle and Kasting, 1986; Hunten et al., 1987). Eq. (A.44) is plotted in Fig. 5 for each f_{H_2} .

It is apparent from Fig. 5 that the diffusion limit is well-obeyed as an upper limit at all levels of irradiation we consider, and it closely approximates the actual escape flux at higher levels of solar irradiation. By contrast the energy-limited flux is ambiguously defined and not obviously well-obeyed, although at low S the slope is correct. The more restricted “energy-limited (XUV)” flux can underestimate escape because it neglects FUV absorbed by CO_2 , whilst the higher “energy-limited (XUV + FUV)”

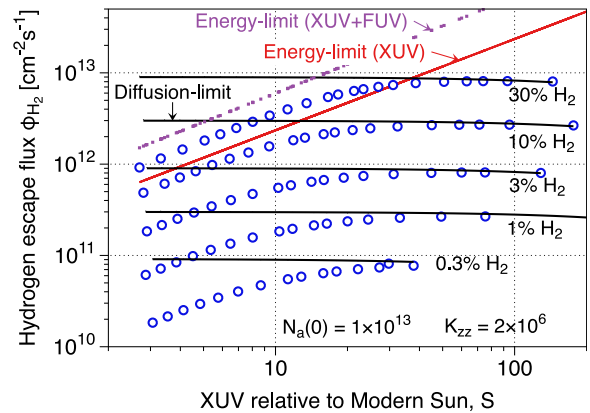


Fig. 5. Hydrogen escape fluxes ϕ_{H_2} from terrestrial CO_2 - H_2 atmospheres as a function of XUV and FUV irradiation S , relative to the modern Sun. Computed ϕ_{H_2} are shown for five H_2 mixing ratios ranging from 0.1% to 30% by volume (blue circles). These are compared to the diffusion-limited flux for the same five hydrogen mixing ratios (horizontal black lines) and to estimates of the energy-limited escape flux, computed either from the EUV energy that hydrogen can absorb (solid red diagonal line) or to the total XUV and FUV energy absorbed by H_2 and CO_2 above the (arbitrary) lower boundary of the model. The computed escape fluxes asymptote to the appropriate diffusion limits at high S . Smaller values of S and f_{H_2} are not shown because two basic assumptions of this study – that thermal conduction can be ignored and that a hydrodynamic description is appropriate, respectively – begin to break down. (For interpretation of the references to color in this figure legend, the reader is referred to the web version of this article.)

flux overestimates escape. Key points are that FUV absorbed by molecules other than H or H_2 can be important (Sekiya et al., 1981), and that both the energy limit and the diffusion limit overestimate hydrogen escape when the hydrogen above the homopause is optically thin to EUV, as discussed by Tian et al. (2005).

Our results in Fig. 5 can be roughly fit by

$$\phi_{\text{H}_2} \approx \frac{2 \times 10^{12} f_{\text{H}_2} S}{\sqrt{1 + 0.006S^2}} \text{ cm}^{-2} \text{ s}^{-1}, \quad (3)$$

good for $f_{\text{H}_2} < 0.2$. Eq. (3) asymptotes to the diffusion-limited flux at large S and asymptotes to an appropriate energy-limited flux for small S .

It is interesting to compare our results to those obtained by time-stepping hydrocode models. In Fig. 6 we compare our results to those obtained by Tian et al. (2005) and Kuramoto et al. (2013). Both hydrocode models explore transonic escape of pure H_2 atmospheres from Earth in response to enhanced levels of incident EUV radiation. Both presume that hydrogen diffusively separates from a lower atmosphere comprising unspecified radiatively active heavy molecules, implicitly CO_2 , although neither model actually includes CO_2 . The lower boundary is held to a fixed temperature and serves as an infinite heat sink. Both hydrocode models include thermal conduction.

The comparison reveals no significant differences in the predicted hydrogen escape fluxes between our shooting

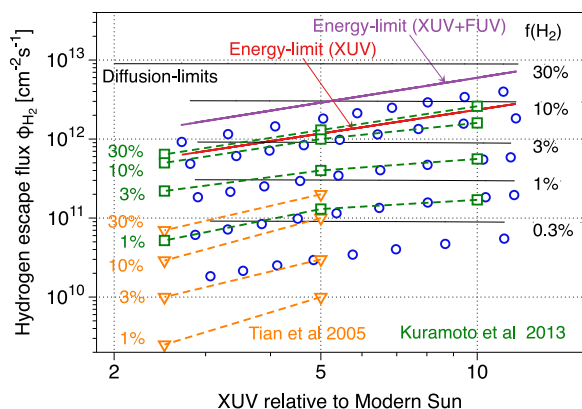


Fig. 6. Comparison between our model (blue circles, from Fig. 5) and published results from two different hydrocodes. The orange triangles denote Tian et al. (2005), the green squares denote Kuramoto et al. (2013); each is plotted for four hydrogen mixing ratios. The Kuramoto et al. (2013) results are quite similar to ours, with minor differences attributable to absorption of solar XUV by CO₂, which is accounted for in our model but neglected by Kuramoto et al. (2013). (For interpretation of the references to color in this figure legend, the reader is referred to the web version of this article.)

code and one of the hydrocodes over the limited EUV range explored by Kuramoto et al. (2013). Both our model and Kuramoto et al. (2013) predict significantly more hydrogen escape than does Tian et al. (2005) for the range of S considered. Why the two hydrocode models differ is not known to us. But if the agreement between our model and Kuramoto et al. (2013) has meaning, the indication is that the physics common to the two models are determining the outcome, and that processes treated differently (e.g., thermal conduction, optical depth, radiative cooling) by the two models are not particularly important to hydrogen escape.

2.5. The magnetic field and the solar wind

In a more realistic setting of Earth, the specific properties of the outer boundary conditions would be determined by the details of the interaction with the solar wind and the weakening of the geomagnetic field with distance (Fig. 7). As most of the bulk properties of the hydrogen wind are determined near the homopause where most of the XUV and FUV radiation is absorbed (shown for the nominal model in Fig. A.14 in Appendix A), the details of the outer boundary are not likely to be very important either to hydrogen escape or to xenon escape.

It is illuminating to compare the ram pressure of the incident solar wind to the ram pressure of hydrodynamically escaping hydrogen and to the strength of the geomagnetic field. The ram pressure of the solar wind is of the order of $\dot{M}_{sw}v_{sw} \approx 10^{-8}$ dynes cm⁻² at Earth. This can be compared to the ram pressure of the hydrodynamic wind $\phi_{H_2}u(r/R_{\oplus})^2$, which in the nominal model is $5 \times 10^{-7}(r/R_{\oplus})^2$ dynes cm⁻². If we presume that \dot{M}_{sw} scales with S , the two rams would butt heads at $r \approx 1.6R_{\oplus}$.

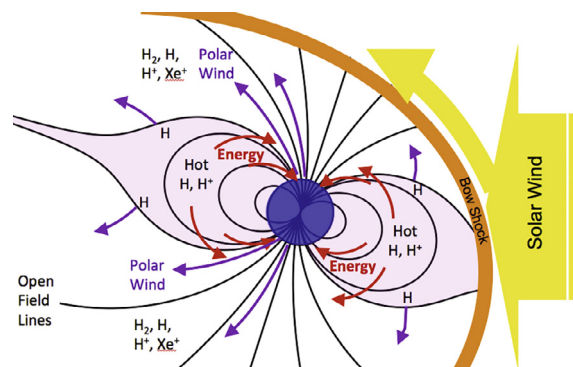


Fig. 7. Geometry of a polar wind in a geomagnetic field. The magnetic field prevents ions from escaping from the tropics. Neutral hydrogen diffuses through the captured ions and eventually escapes, but escape is enough impeded that the corona becomes rather dense and very hot. By contrast, the geomagnetic field does not prevent ion escape along the open polar field lines, and as a consequence of free escape the gas remains relatively cool while also retaining the capacity to drag Xe ions with it. The flow of energy from the hot dense trapped corona to the poles has the potential of greatly enhancing the effective S pertinent to the polar wind. The solar wind complicates the flow but, regarded over the globe as a whole, is more likely to aid escape than to impede it.

The more pertinent comparison is to the much greater strength of Earth's magnetic field for $r < 4R_{\oplus}$. A dipole field falls off as $(0.25B_{\oplus}^2/\pi)(R_{\oplus}/r)^6 \approx 1.5 \times 10^{-7}(6R_{\oplus}/r)^6$ dynes cm⁻² using $B_{\oplus} = 0.31$ Gauss for Earth today. These crude estimates suggest that the solar wind will play a major role in determining the outer boundary conditions in the absence of a geomagnetic field, but would have less consequence for hydrodynamic escape channeled along magnetic field lines in the presence of a field, even one as small as $0.1B_{\oplus}$. Whether early Earth had a significant magnetic field is debated (Ozima et al., 2005; Tarduno et al., 2014; Biggin et al., 2015; Weiss et al., 2018).

3. XENON ESCAPE AS ION

We use the solutions for H escape obtained in Section 2 and Appendix A to construct models of Xe escape. We assume that xenon is a trace constituent that has no effect on the background atmosphere. Our purpose is to determine the minimum requirements for Xe to escape, which is equivalent to determining whether Xe⁺ escape is possible. We therefore focus on Xe⁺. In this section we first discuss how we compute Xe⁺ escape for a given atmosphere and level of solar irradiation. Some general considerations pertinent to Xe⁺ escape are outlined in Fig. 8.

3.1. Xenon chemistry

Xenon can be directly photo-ionized (Huebner et al., 1992),



and it can be ionized by chemical reactions with other ions. In the idealized H-H₂-CO₂ atmosphere, the chief possibili-

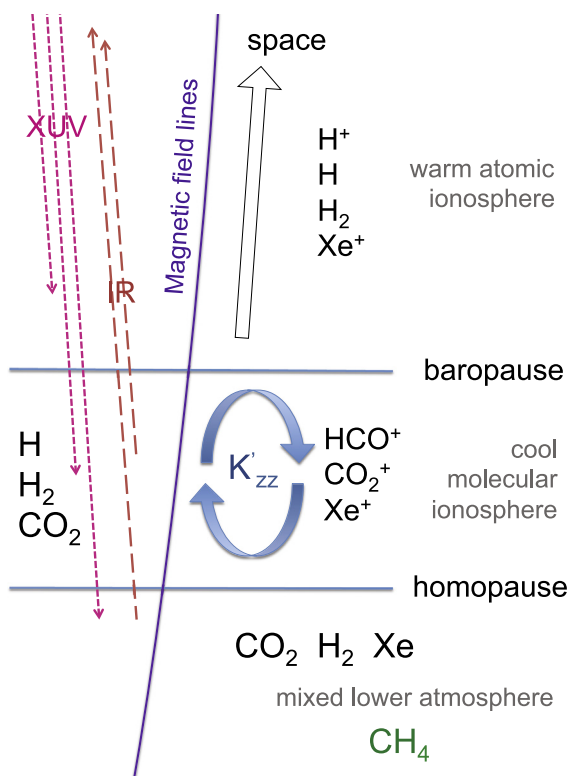
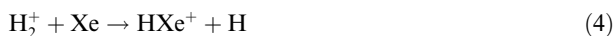


Fig. 8. Structure of the CO₂-H₂ upper atmosphere pertinent to Xe escape. There are three layers: a mixed lower atmosphere; a relatively thin cool molecular ionosphere with HCO⁺ and CO₂⁺ the major ions; and a greatly distended outflowing upper ionosphere dominated by hydrogen and its ions. The divisions between the layers are marked homopause and “baropause.” The latter denotes the highest altitude where heavy elements are important. There are three barriers to Xe escape as an ion. First, ion escape is blocked by a geomagnetic field save near the poles where field lines open into space. Second, hydrogen escape from the atomic ionosphere must be vigorous enough that Xe ions are swept away. Quantifying this requirement determines what S and f_{H_2} must be for Xe escape. Third, Xe ions need to be transported through the molecular ionosphere to the baropause, probably by vertical movements of molecular ions themselves. This too depends on S . We model this in 1-D as an ion eddy diffusivity K'_{zz} , which we treat as a third parameter in the model.

ties are reactions of neutral Xe with the primary ions H⁺, H₂⁺, and CO₂⁺. The charge exchange reaction with CO₂⁺ (Anicich and Huntress, 1986)



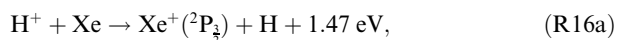
is fast and important at low altitudes where CO₂ is photoionized. The reaction of Xe with H₂⁺



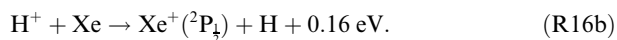
occurs but it is not a source of Xe⁺ because the XeH⁺ ion dissociatively recombines; we ignore it.

Charge exchange with H⁺ presents the most interesting case. In general, charge exchange reactions between light atoms are slow save when the reaction is nearly resonant

(Huntress, 1977). The reaction into the Xe⁺ ground state is far from resonance,



and is therefore unlikely to be fast. On the other hand, Xe⁺ has a low-lying electronically-excited state for which charge exchange is exothermic yet not far from resonance (Shakeshaft and Macek, 1972),

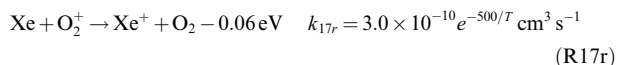
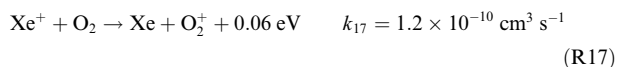


There appear to be no relevant measurements, while a calculation by Sterling and Stancil (2011) does not take into account fine structure and thus uses large asymptotic energy separation between different charge arrangements. We therefore revisited the calculation of the rate of R16b, as described in Appendix B. An empirical curve fit to k_{16b} good for temperatures between 50 and 10⁵ K is

$$k_{16b} = 3.83 \times 10^{-8} T^{0.386} \exp(-55.8/T^{0.326}) \quad \text{cm}^3 \text{ s}^{-1}. \quad (5)$$

The rate k_{16b} is of the order of 10⁻¹¹ cm³ s⁻¹ at 300 K and 10⁻¹⁰ cm³ s⁻¹ at 800 K, rates that are fast enough that charge exchange becomes an important source of Xe⁺ at high altitudes where H⁺ is abundant. The reverse of R16b is 0.16 eV endothermic and therefore smaller than k_{16b} by a factor of the order of $e^{-1860/T}$, which ensures that the excited Xe⁺(²P_{1/2}) ion relaxes radiatively or collisionally to the ground state before it can lose its charge.

The Xe⁺ ion once made does not react with H, H₂, or CO₂. A potentially important reaction at lower altitudes is the nearly resonant charge exchange with O₂ (Anicich, 1993)



R17r can be a source of Xe⁺ in an atmosphere without much O₂, because O₂⁺ can be abundant in a CO₂ atmosphere without O₂ being abundant (cf., Venus; Fegley, 2003), but R17 becomes an important sink of Xe⁺ when O₂ is abundant.

Xe⁺ also reacts with small hydrocarbons other than CH₄ (e.g., C₂H₂ and C₂H₆, Anicich, 1993) to form HXe⁺, which then dissociatively recombines. This suggests that Xe escape could be suppressed when conditions favor formation of high altitude hydrocarbon hazes (as seen on Titan, Triton, and Pluto). Organic hazes have been a topic of extensive speculation for Archean Earth (Domagal-Goldman et al., 2008; Zerkle et al., 2012; Hébrard and Marty, 2014; Arney et al., 2016; Izon et al., 2017). It might be tempting to link a possible hiatus in Xe isotopic evolution noted by Avice et al. (2018) between 3.2 Ga and 2.7 Ga to Archean organic hazes. It has recently been shown that isotopically ancient Xe was trapped in ancient organic matter on Earth (Bekaert et al., 2018); however, it is not yet known if the trapping was by a high altitude haze.

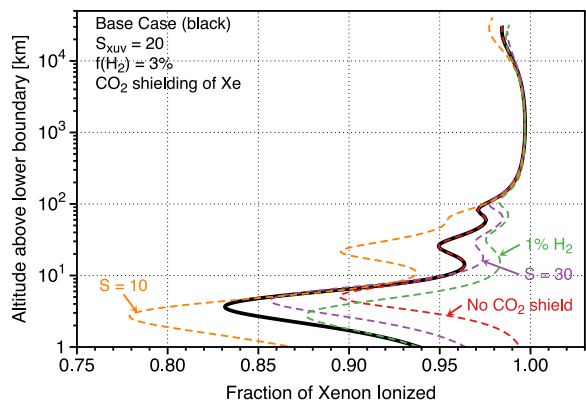
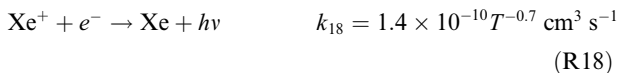


Fig. 9. Equilibrium fractional ionization of xenon for several exemplary cases. The broken curves are each labeled according to how they differ from the base case. Altitude is measured from an arbitrary lower boundary where the total density $n(r_0) = 1 \times 10^{13} \text{ cm}^{-3}$. The variant “no CO₂ shield” (red dashed line) presumes that Xe is photo-ionized through windows in CO₂’s opacity. (For interpretation of the references to color in this figure legend, the reader is referred to the web version of this article.)

Radiative recombination of Xe⁺ is the unavoidable sink. We assume that it is neither much faster nor much slower than radiative recombination of H⁺,



In Fig. 9 we show the equilibrium ionization computed from

$$k_{18}x_jn_e = J_{\text{Xe}}n_j + k_{15}n_3n_j + k_{16b}x_1n_j, \quad (6)$$

where we have denoted the number densities of different Xe and Xe⁺ isotopes by n_j and x_j , respectively. Fig. 9 plots the fractional ionization $x_j/(n_j + x_j)$ in the nominal model and several variants on the nominal model. Variants include $f_{\text{H}_2} = 0.01$, $S = 10$, and $S = 30$. “CO₂ shielding” refers to the overlap between Xe’s absorption and CO₂’s absorption, both of which are spiky between 91.2 and 102.3 nm; the base case presumes that CO₂’s absorption and Xe’s absorption fully overlap, so that CO₂ shields Xe from photo-ionization. The variant labeled “no CO₂ shield” presumes no spectral overlap between CO₂ and Xe, in which case Xe is photo-ionized through windows in CO₂’s opacity. In all cases Xe’s equilibrium ionization typically exceeds 90%.

3.2. Xenon transport

The forces acting on Xe⁺ ions are the collisions with hydrogen and H⁺ that push Xe⁺ outwards, the collisions with CO₂ that block it, the Coulomb interactions with molecular ions that are not escaping, the electric field that tethers the electrons to the ions, and the force of gravity that pulls the Xe ions back to Earth. To these we add eddy mixing as described in Appendix B.

The molecular ions, here CO₂⁺ and HCO⁺, present a barrier to Xe⁺ escape, because Xe⁺ is strongly coupled to them

by the strong Coulomb interaction and the relatively high reduced mass (compared to H⁺) that makes collisions proportionately more effective at transferring momenta. Molecular ions dominate Xe⁺ transport in the nominal model from the homopause at 10 km above the lower boundary to the baropause at 80 km above the lower boundary, Fig. B.17. Where the molecular ions flow upward, Xe⁺ is carried up with them and may gain the opportunity to escape; where the ions flow downward or sideways or sit quietly, Xe⁺ cannot escape. On Earth today at relevant thermospheric altitudes, vertical winds of the order of 10 to 20 m s⁻¹ are often observed, and often sustained for an hour or more (Ishii, 2005; Larsen and Meriwether, 2012). We will assume that these vertical velocities, which are measured in the Doppler shifts of narrow forbidden lines of atomic oxygen (Ishii, 2005), are also pertinent to the molecular ions. These winds imply rapid and considerable vertical transport. An upward velocity of 20 m/s sustained for an hour suffices to lift Xe⁺ by 70 km, which is enough to carry it through the molecular ionosphere to where it can be handed off to protons and hydrogen escape. The molecular ions themselves cannot get very far, because the typical lifetime against dissociative recombination is only ~ 10 s. The Xe ion’s lifetime could be much longer, possibly as long as 10 days, its lifetime against radiative recombination. In all likelihood the reaction with O₂ is the actual sink in a CO₂-rich atmosphere. For Xe⁺ to last an hour, the O₂ density must be less than $2 \times 10^6 \text{ cm}^{-3}$, ~ 1 ppm at the homopause. The O₂ sink would be smaller in an N₂-CO₂-H₂ atmosphere and negligible in an N₂-CO-H₂ atmosphere.

The usual method of describing vertical transport in a 1-D model is through an eddy diffusivity K_{zz} that acts to reduce the gradient of the mixing ratio. As a practical matter eddy diffusion is straightforward to implement in a 1-D model and it is well-behaved numerically. Eq. (A.30) in Appendix A provides an effective definition.

Here we will define a K'_{zz} that acts on the ions at altitudes above the neutral homopause. The observed vertical winds and timescales, $v = 10 \text{ m/s}$ and $t = 4000 \text{ s}$, imply $K'_{zz} \sim v^2 t \approx 4 \times 10^9 \text{ cm}^2 \text{ s}^{-1}$. Another way to construct K'_{zz} is as turbulence. In this case K'_{zz} scales as the product of the sound speed and a length scale, multiplied by a scaling factor α . This scaling is used in the ubiquitous α -disk model of astrophysical accretion disks, with the scale length equated to the scale height. The models work best with α of the order of 0.1 to 0.4 (King et al., 2007). Using this prescription, a turbulent K'_{zz} might be of the order of $1 \times 10^9 - 4 \times 10^9 \text{ cm}^2 \text{ s}^{-1}$. Turbulence with $\alpha > 1$ implies supersonic winds, which is regarded as unsustainable. On the other hand, concerted motions could yield higher K'_{zz} than turbulence.

We will use $K'_{zz} = 4 \times 10^9 \text{ cm}^2 \text{ s}^{-1}$ for the ions as a nominal model, but it should be noted that such a high value of K'_{zz} vastly exceeds the neutral eddy diffusivity $K_{zz} \sim 10^6 \text{ cm}^2 \text{ s}^{-1}$ used in contemporary thermospheric chemistry modeling (Salinas et al., 2016).

In addition to drag and gravity, the electric field that tethers the ions to the free electrons has to be big enough

to balance half the weight of the ion, such that the sum of the masses of the electron and the ion is $(m_i + m_e)/2 \approx m_i/2$. The electric field generated by HCO^+ (29 amu) would therefore produce an upward force of $14.5m_{\text{Hg}}$, which is a relatively small correction for an ion as massive as Xe^+ , but quite big for light ions like H^+ and O^+ . We include the electric force on Xe^+ as a modification of the gravitational force by computing the mean mass of the ions μ^+ .

The governing equation for Xe^+ escape is developed in Appendix B as Eq. (B.14). Eq. (B.14) is a differential equation for the Xe ion velocity $v_j(r)$ that is solved by the shooting method. The Xe ion velocity $v_j(r)$ is integrated upward from the lower boundary for all nine Xe isotopes. The lower boundary velocity $v_j(r_0)$ is bounded by 0 and by the hydrogen velocity $u(r_0)$ (i.e., Xe cannot escape more easily than hydrogen). The velocity $v_j(r_0)$ at the lower boundary is iterated until either $v_j(r) \rightarrow u(r)$, in which case Xe^+ escapes, or $v_j(r) \rightarrow 0$, in which case Xe^+ is hydrostatic and does not escape.

3.3. Some numerical results

We describe our results in terms of an escape factor α_j of isotope j with respect to hydrogen. The escape factor is equal to the ratio of the velocity of isotope j to the velocity of hydrogen at the lower boundary,

$$\alpha_j \equiv \frac{\phi_j}{n_j(r_0)} \div \frac{\phi_{\text{H}_2}}{n_{\text{H}_2}(r_0)} = \frac{v_j(r_0)}{u(r_0)}. \quad (7)$$

The escape factor can be thought of as the relative probability that an atom of ^jXe escapes compared to an atom of hydrogen.

We could define an analogous escape factor between two isotopes by taking the ratio of α_i to α_j , but it is more natural in hydrodynamic escape to define a “fractionation factor” as the difference between α_i and α_j ,

$$\alpha_{ij} \equiv \alpha_j - \alpha_i. \quad (8)$$

We will evaluate α_{ij} for $j = 130$ and $i = 131$.

Fig. 10 shows how the escape factor α_j varies as a function of irradiation S for the nominal model ($f_{\text{H}_2} = 0.03, K'_{zz} = 4 \times 10^9 \text{ cm}^2 \text{ s}^{-1}$) and some variants. The minimum irradiation for significant Xe^+ escape is $S > 10$, comparable to what is expected from the average Sun ca 3.5 Ga. At very high levels of irradiation, Xe escape decreases because the Coulomb cross section between ions decreases at high temperatures.

Fig. 11 shows how the Xe escape factor α_j varies as a function of hydrogen mixing ratio f_{H_2} for the nominal model ($S = 20, K'_{zz} = 4 \times 10^9 \text{ cm}^2 \text{ s}^{-1}$) and some variants. The minimum hydrogen mixing ratio at the homopause for significant Xe^+ escape is $\sim 0.4\%$, achievable when both S and K'_{zz} are very large; at the lower levels of irradiation expected during the Archean, the lower bound on f_{H_2} is $\sim 1\%$.

Fig. 12 shows how the Xe escape factor α_j depends on the modeling parameter K'_{zz} for the nominal $S = 20$ and a

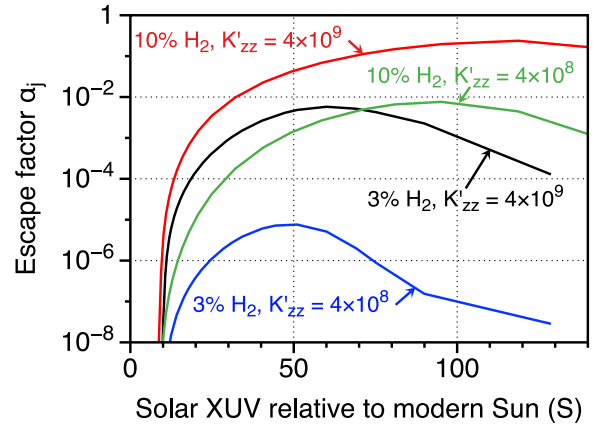


Fig. 10. Xenon escape factors α_j for $j = 130$ as a function of solar XUV irradiation S for selected values of K'_{zz} and f_{H_2} . Xenon escape requires $S > 10$, a level of solar activity expected of the active Sun before 2.5 Ga.

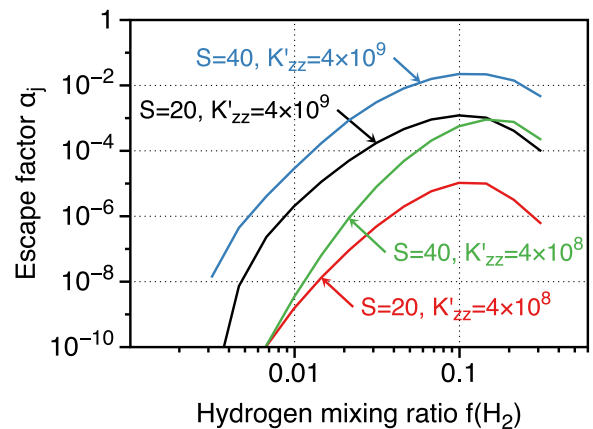


Fig. 11. Xenon escape factors α_j for $j = 130$ as a function of hydrogen mixing ratio for some selected values of K'_{zz} and S . The smallest hydrogen mixing ratio where Xe can escape is about 0.4%, and this only for the most favorable choices of K'_{zz} and S . Significant Xe escape in the Archean probably requires $f_{\text{H}_2} > 0.01$.

variety of hydrogen mixing ratios. The modeling parameter K'_{zz} describes vertical transport by ions through the lower molecular ionosphere as a diffusivity, a form well-suited to a 1-D model. As discussed above, a plausible upper bound on K'_{zz} is of the order of $c_s H_{\text{CO}_2} \approx 1 \times 10^{10} \text{ cm}^2 \text{ s}^{-1}$ if K'_{zz} derives from turbulence; K'_{zz} could be larger if transport is by large scale circulation, and it could be much smaller if transport were more akin to that amongst the neutrals near the neutral homopause.

Fig. 13 summarizes Xe^+ fractionation factors α_{ij} as contours on the $S - f_{\text{H}_2}$ plane, with the three panels corresponding to three values of K'_{zz} . The figure graphically illustrates the tradeoffs between S, f_{H_2} , and K'_{zz} . Bounds on f_{H_2} depend on K'_{zz} . The right hand panel shows that if K'_{zz} is too small, Xe escape would be difficult in the Archean where $S < 20$, while the left hand panel of Fig. 13 sets K'_{zz} so high that the mixing length would have to greatly exceed

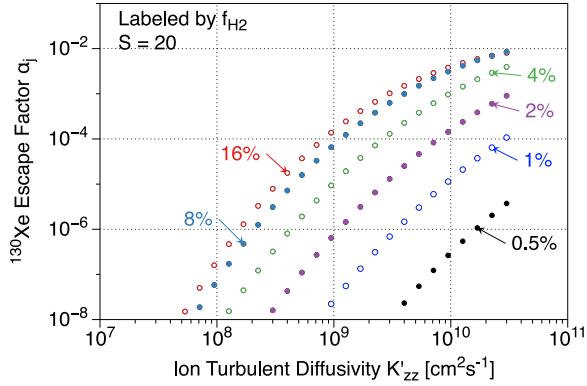


Fig. 12. Variation of Xe escape from a CO₂-H₂ atmosphere as a function of the modeling parameter K'_{zz} for several different f_{H_2} for “nominal” value of $S = 20$. A plausible upper bound on $K'_{zz} \sim 1 \times 10^{10} \text{ cm}^2 \text{ s}^{-1}$ if K'_{zz} derives from turbulence; it could be larger if transport is by large scale circulation, and it would be much smaller if transport were more akin to that amongst the neutrals. The figure illustrates the tradeoff between K'_{zz} and f_{H_2} .

the scale height, which is probably not possible unless the flow were organized by the geomagnetic field, for which characteristic length scales are long. The middle path is consistent with Xe escape in the Archean provided that the atmosphere contains $> 1\%$ hydrogen (or $> 0.5\%$ methane).

4. FRACTIONATION

Escape factors and fractionation factors are snapshots in time. The observables – the isotopic fractionation and total xenon loss – are integrated quantities that depend on the cumulative histories of the solar XUV irradiation $\int S(t)dt$, the mass and composition of the atmosphere, the presence or absence of a planetary magnetic field, and probably several other things that we haven’t addressed.

A convenient way to describe the fractionation between two isotopes ^iXe and ^jXe is to compare the ratio of their relative abundances at a later time t_B to their relative abundances at an earlier time t_A ,

$$\xi_{ij}(t_A, t_B) \equiv \frac{N_i(t_B)}{N_i(t_A)} \div \frac{N_j(t_B)}{N_j(t_A)}, \quad (9)$$

where N_j represents the total (column) reservoir of isotope j (number per cm^2). When applied to hydrodynamic escape, the fractionation $\xi_{ij}(t_A, t_B)$ describes the relative depletion of isotope i compared to isotope j . We will take U-Xe (Pepin, 1991, 2006) as the initial composition at t_A ; our results are insensitive to this choice. In hydrodynamic escape, the rate of change of $\xi_{ij}(t)$ can be expressed in terms of hydrogen escape,

$$\frac{1}{\xi_{ij}} \frac{\partial \xi_{ij}}{\partial t} = \frac{1}{N_i} \frac{\partial N_i}{\partial t} - \frac{1}{N_j} \frac{\partial N_j}{\partial t} = \frac{\phi_j}{N_j} - \frac{\phi_i}{N_i} = -\frac{\phi_{\text{H}_2}}{N_{\text{H}_2}} \alpha_{ij}. \quad (10)$$

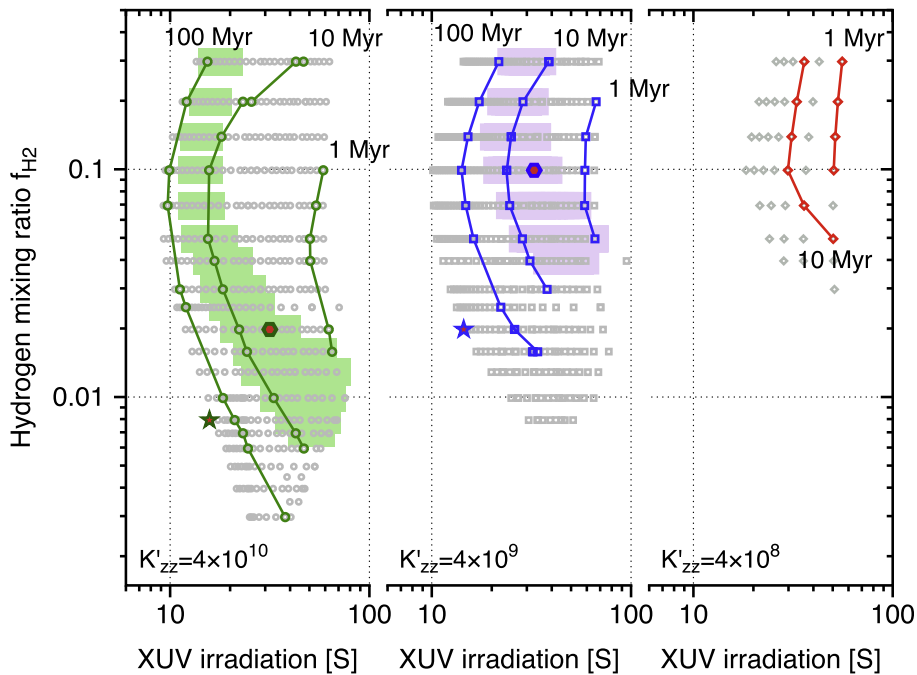


Fig. 13. Xenon escape as a function of irradiation S and hydrogen mixing ratio f_{H_2} , for three values of eddy diffusivity K'_{zz} that correspond to different rates of transport through the molecular ion barrier. The middle panel ($K'_{zz} = 4 \times 10^9 \text{ cm}^2 \text{ s}^{-1}$) is the nominal case. The high value $K'_{zz} = 4 \times 10^{10} \text{ cm}^2 \text{ s}^{-1}$ in the left-hand panel exceeds what could plausibly be attributed to turbulence. The gray symbols mark out regions of the $S - f_{\text{H}_2}$ plane where xenon escape is significant. The shaded regions encompass models that at uniform conditions can simultaneously reproduce both Xe’s mass fractionation and depletion. The contours are labeled by how long it takes (elapsed time) for fixed conditions to generate the observed Xe isotopic fractionation if Xe escape is global. It takes proportionately longer if Xe escape is channeled through polar apertures; i.e., the curve marked “10 Myr” corresponds to 100 Myrs if escape is restricted to 10% of Earth’s area. The stars and hexagons mark exemplary cases singled out for discussion in the text.

The fractionation ξ_{ij} between isotopes ^jXe and ^iXe is the integral

$$\ln \{ \xi_{ij}(t_A, t_B) \} = - \int_{t_A}^{t_B} \frac{\phi_{\text{H}_2}}{N_{\text{H}_2}} \alpha_{ij}(t) dt. \quad (11)$$

Similarly, the total loss or depletion ξ_j of the isotope ^jXe can be defined

$$\xi_j(t_A, t_B) \equiv \frac{N_j(t_B)}{N_j(t_A)}, \quad (12)$$

which can also be described by an integral over hydrogen escape

$$\ln \{ \xi_j(t_A, t_B) \} = - \int_{t_A}^{t_B} \frac{\phi_{\text{H}_2}}{N_{\text{H}_2}} \alpha_j(t) dt. \quad (13)$$

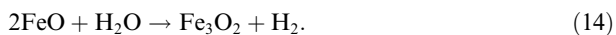
Eq. (11) for fractionation ξ_{ij} and Eq. (13) for depletion ξ_j presume that almost all of Earth's xenon is and was in the atmosphere; i.e., it is presumed that the columns N_j faithfully represent the global inventories.

4.1. Constraints

Xenon directly places two constraints on escape. The mass fractionation of the isotopes, ξ_{ij} – roughly 4‰ per amu, about half of this taking place after 3.5 Ga – is the more secure and the more telling, so it takes primacy. As we shall see, the most important aspect of this constraint is that escape was drawn out over one to two billion years, which is why Xe escape implies the loss of a great deal of water.

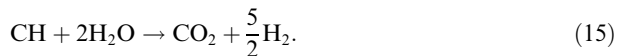
The second constraint is on the total xenon escape, ξ_j . Total escape conflates the apparent 4–20-fold depletion with respect to Kr in meteorites (Fig. 1) with the missing daughter products of spontaneous fission of ^{244}Pu ; it also lacks the historic record of evolution we have for the isotopes. Because Earth's original U-Xe is not found in meteorites, the depletions with respect to Kr in meteorites are at best rough guides to what the true depletion might be. Earth retains about 20% of the Xe spawned by spontaneous fission of ^{244}Pu (80 Myr half-life; Pepin, 1991, 2006; Tolstikhin et al., 2014). There are enough uncertainties in Earth's U abundance and original Pu/U ratio, and in possible nonfractionating loss mechanisms left (like impact erosion) that we will simply treat $\xi_j \approx 0.25$ as a best guess.

A third constraint is the total oxidation of the Earth. Hydrogen escape can oxidize the Earth from an initially reduced, Moon-like state (Sharp et al., 2013). An upper bound on cumulative oxidation is obtained by adding up the ferric iron and the CO_2 contents of Earth. To first approximation, the Fe_2O_3 inventory in the MORB-source mantle (> 0.3 wt%, Cottrell and Kelley, 2011) can be balanced with the oxygen from the escape of ~ 1 ocean of water,



Dauphas and Morbidelli (2014) estimate from CO_2/Nb systematics that there are 3.4×10^{22} moles of carbon on Earth (the majority in the mantle). Carbon isotopes suggest that 80% of Earth's C is in CO_2 . Although some carbon was

accreted by Earth in the form of CO_2 (as ice in comets or as carbonate minerals in meteorites), most of it probably accreted in reduced form, which we idealize as CH. The stoichiometry of carbon oxidation by H_2O is



If we assume that 20% of Earth's C was directly accreted as CO_2 and the other 80% as CH, the oxidation of carbon on Earth corresponds to the oxygen extracted from ~ 0.3 oceans of water. As there are alternative stories to explain how the mantle became oxidized (Frost and McCammon, 2008), escape of one or two oceans of water can be regarded as an upper bound.

A fourth constraint stems from the kinetics of Earth's oxidation. If the escaping H_2 comes from H_2O , something must be oxidized and exported to the mantle, which can be rate-limiting. It is illustrative to consider a rough upper bound set by oxidation of ferrous to ferric iron. This includes weathering of continents and seafloor. For the former, presume that continents of modern mass and 7% Fe were built, eroded, weathered, and subducted on a 1 Gyr time scale, with 100% conversion of Fe^{+2} to Fe^{+3} . This would correspond to an average H_2O sink of 7×10^{12} moles yr^{-1} . For the latter, presume that the upper 1% of the seafloor was oxidized and that the mantle turned over in 1 Gyr. This corresponds to an average H_2O sink of 1.4×10^{13} moles yr^{-1} . The latter can be compared to an Fe^{+2} source of $0.6 - 1.2 \times 10^{13}$ moles yr^{-1} estimated by scaling modern midocean ridge hydrothermal fluxes (Ozaki et al., 2018). Note that Ozaki et al. (2018) infer much higher total Fe^{+2} fluxes of order $7 - 21 \times 10^{13}$ moles yr^{-1} , most of which is biologically recycled. The high recycled flux maps to high CH_4 production, which suggests that H_2 levels could change dramatically in response to biological forcing; e.g., blooms.

Summed, the *de novo* weathering source of H_2 probably did not exceed 2×10^{13} moles yr^{-1} , or 0.25 oceans per Gyr. The equivalent H_2 escape flux – 8×10^{10} molecules $\text{cm}^{-2} \text{s}^{-1}$ in photochemical units – corresponds to hydrogen mixing ratios $\leq 1\%$ in a 1 bar Archean atmosphere, and is probably insufficient to support Xe escape unless the atmosphere were substantially thinner than 1 bar, or the ferrous iron oxidation rate varied significantly in response to climate fluctuations, variations in the biological production of CH_4 , changes in tectonic style, or episodic continent building.

Two other sources of H_2 are worth mentioning. A big mantle source of H_2 and other reduced gases may be plausible in the Hadean while metallic iron was still extant but is less likely in the Archean when the mantle appears to have been only modestly more reduced than today. A more exotic possibility is that H_2 and other reduced gases were injected episodically into the atmosphere from degassing of reduced impacting bodies (Kasting, 1990; Hashimoto et al., 2007; Schaefer and Fegley, 2010). A 10^{21} g chondritic body, comparable to the bigger Archean impact events documented by Lowe and Byerly (2018), on reacting with Earth's oceans would inject of order 3×10^{18} moles of H_2

into the atmosphere (0.02 bars), enough to support a burst of Xe escape.

The D/H ratio of Earth may provide some support for the hypothesis that Earth lost an ocean or more of water. Zahnle et al. (1990) found that the escape factor for HD with respect to H₂ in diffusion-limited hydrogen escape with $f_{\text{H}_2} \ll f_{\text{CO}_2}$ is $\alpha_{\text{HD}} \approx 0.8$. The resulting Rayleigh fractionation of the water that remains on Earth leads to a modest enhancement of the D/H ratio,

$$\frac{\text{D}/\text{H}(t_B)}{\text{D}/\text{H}(t_A)} = \left(\frac{M_{\text{H}_2\text{O}}(t_A)}{M_{\text{H}_2\text{O}}(t_B)} \right)^{1-0.8} \quad (16)$$

If for example Earth lost two oceans of water by diffusion-limited hydrogen escape, the resulting D/H enrichment would be of the order of $3^{0.2} = 1.25$. The predicted 25% enrichment in D/H is less than the $\sim 40 - 60\%$ difference between Earth's D/H and the D/H ratios measured in most carbonaceous chondrites, and it is small compared to the scatter between the measured D/H ratios in the array of known possible sources of Earth's water (Alexander et al., 2012). Pope et al. (2012) reported that the D/H ratio of seawater at 3.8 Ga was 2.5% lighter than today, which corresponds to the loss of about 13% of an ocean according to Eq. (16).

4.2. Example 1

To quantify concepts, consider first an order of magnitude estimate for Archean conditions, using only the fractionation ξ_{ij} as a constraint. Assume that fractionation of 2% per amu took place between 3.5 Ga and 2.5 Ga (Fig. 3), and assume a constant integrand in Eq. (11), which effectively means holding α_j constant,

$$\ln \{ \xi_{ij} \} = 0.02 \approx \frac{\phi_{\text{H}_2}}{N_{\text{H}_2}} \alpha_{ij} (t_B - t_A). \quad (17)$$

Using Eq. (3), Eq. (17) evaluates to

$$\alpha_{ij} = 5 \times 10^{-7} p_{\text{atm}} \left(\frac{1 \text{ Gyr}}{t_A - t_B} \right) \quad (18)$$

where p_{atm} is the total atmospheric pressure in bars and $N_a = 1.4 \times 10^{25} \text{ cm}^{-2}$ for 1 bar of CO₂. For the particular case with $f_{\text{H}_2} = 0.02$ and $K'_{zz} = 4 \times 10^9 \text{ cm}^2 \text{ s}^{-1}$, the inferred $\alpha_{ij} = 5 \times 10^{-7}$ corresponds to $S = 15$ and $\alpha_j = 5 \times 10^{-6}$. This case is marked by the blue star in the middle panel of Fig. 13. Total Xe loss is only $\xi_j = 0.67$, which means that Earth loses only one-third of its Xe between 3.5 and 2.5 Ga. In global escape, the required hydrogen loss (expressed as equivalent water) is

$$M_{\text{H}_2\text{O}} = 1.3 \times 10^{13} m_{\text{H}_2\text{O}A_{\oplus}} \left(\frac{f_{\text{H}_2}}{0.02} \right) (t_B - t_A) = 1.2 \times 10^{24} \text{ grams} \quad (19)$$

which is 0.86 oceans of water (1 ocean is $1.4 \times 10^{24} \text{ g}$). This is probably too much mantle oxidation after 3.5 Ga, given that we have not addressed the first billion years and the other half of xenon's fractionation. With the same $S = 15$,

the extreme $K'_{zz} = 4 \times 10^{10} \text{ cm}^2 \text{ s}^{-1}$ works with $f_{\text{H}_2} = 0.008$, which corresponds to 0.35 oceans lost during the Archean. This case is marked by the green star in the left panel of Fig. 13. In both cases, the trickle of Xe escape is very close to no Xe escape at all. In a more realistic scenario, $\alpha_{ij} \gg 5 \times 10^{-7}$ where and when Xe escapes, averaged with a more typical state in which Xe does not escape ($\alpha_j = \alpha_{ij} = 0$).

4.3. Example 2

Our second example is constrained to simultaneously match both the fractionation ξ_{ij} and the depletion ξ_j . In the special case of constant integrands in Eqs. (11) and (13), the fractionation ξ_{ij} and the depletion ξ_j are related by

$$\frac{\alpha_j}{\alpha_{ij}} = - \frac{\ln(\xi_j)}{\ln(\xi_{ij})} \approx - \frac{\ln(0.25)}{0.04} \approx 35. \quad (20)$$

Eq. (20) is effectively Rayleigh fractionation. Models with $25 < \alpha_j/\alpha_{ij} < 45$ are marked out in shades of color in Fig. 13. In general, these solutions require high rates of escape, driven by high f_{H_2} or high S or both.

Two models that fit these constraints are marked by hexagons in Fig. 13, one with $K'_{zz} = 4 \times 10^9 \text{ cm}^2 \text{ s}^{-1}$ and $f_{\text{H}_2} = 0.10$ (middle panel), the other with $K'_{zz} = 4 \times 10^{10} \text{ cm}^2 \text{ s}^{-1}$ and $f_{\text{H}_2} = 0.02$ (left panel). Both use a relatively high solar EUV irradiation of $S = 30$. Both examples give $\alpha_j = 1 \times 10^{-2}$ and $\alpha_{ij} = 2.5 \times 10^{-4}$. For uniform conditions, the time scale ($t_B - t_A$) to evolve Xe fractionation is just 3 Myrs if escape is global and 30 Myrs if escape is channelled through polar windows open over 10% of Earth. The hydrogen lost globally in 30 Myr is only 0.05 oceans with $K'_{zz} = 4 \times 10^{10}$, or 0.25 oceans with $K'_{zz} = 4 \times 10^9$. This could be the whole story if hydrogen were present only in brief episodes that sum to 30 Myrs, scattered over the two billion years during which Xe fractionation took place.

To quantify the previous statement, consider a pulse of hydrogen into the atmosphere. From Eq. (3), escape goes as

$$\frac{dN_{\text{H}_2}}{dt} \approx \frac{2 \times 10^{12} S}{\sqrt{1 + 0.006S^2}} \frac{N_{\text{H}_2}}{N_A}. \quad (21)$$

Eq. (21) predicts that f_{H_2} exponentially decays on the time scale

$$\tau_{\text{H}_2} = \frac{N_A \sqrt{1 + 0.006S^2}}{2 \times 10^{12} S} \frac{N_{\text{H}_2}}{N_A} \approx 3 \times 10^4 \text{ years} \quad (22)$$

for $S > 10$ and 1 bar of CO₂. It takes ~ 1000 episodes (summing to 30 Myrs total if channelled through polar windows that open over 10% of Earth) that each raised f_{H_2} to 10% (or 2% for $K'_{zz} = 4 \times 10^{10}$) to account for Xe escape. Of course there would also be many more hydrogen excursions too small to drive Xe escape, or that took place at an inopportune time when S was too small, and it will be the number and magnitude of these other events that determines how much hydrogen escapes in total.

4.4. Example 3

Consider finally a schematic example that more explicitly invokes the geomagnetic field. This is the scenario illustrated schematically in Fig. 7. The magnetic field partitions escape into two regimes. Near Earth any plausible geomagnetic field is much stronger than the hydrodynamic wind, and therefore controls it. This ordering of strengths is determined by comparing the magnetic pressure $B^2/4\pi$ of the field to the ram pressure $\phi_{\text{H}_2} m_{\text{H}_2} u$ of the wind. Because the strength of a dipole field drops as r^{-6} , at large distances the polar wind eventually overcomes the field and stretches the field radially. The polar field lines open out to space and both ions and neutrals can escape. This is the situation we have been modeling.

The equatorial region, however, is quite different. Here the field lines remain closed and ions, which cannot cross the field lines, cannot escape. The result is a relatively hot and dense quasi-static partially ionized plasma that exerts a pressure limited only by the native strength of the geomagnetic field. Although neutrals can still escape by diffusing through the ions, escape is inhibited and is probably restricted to H and He. A detailed examination of the inflated magnetosphere is beyond the scope of this study; what is important here is that (i) Xe cannot escape through the equatorial magnetosphere because ions are trapped, and (ii) there will be a flow of energy from the hot dense equatorial magnetosphere to the cooler, sparser, but free-flowing polar wind.

As it pertains to Xe escape, the net effect of a more realistic geomagnetic geometry is to subvert the constraint on S in the Archean that would otherwise be inferred from solar analogues. If we take the polar wind to be described by the constant $f_{\text{H}_2} = 0.02$, high K'_{zz} case from Example 3, the total hydrogen escape through the polar windows would be 0.33 oceans over 2 billion years. If away from the poles we take $S = 6$, typical of the mid-Archean, the total equatorial hydrogen loss with constant f_{H_2} over 2 Gyr would be ~ 1.5 ocean. In this scenario xenon escape occurs exclusively at the poles and only at rare times when S was abnormally large, while hydrogen escape is constant from an atmosphere that is always 2% hydrogen.

5. DISCUSSION

In this study we have argued that Xe escaped Earth as an ion and we have quantified the hypothesis in the context of a restricted range of highly idealized models of diffusion-limited hydrodynamic hydrogen escape from $\text{CO}_2\text{-H}_2$ atmospheres in the absence of inhibition by a magnetic field. These atmospheres develop cold lower ionospheres dominated by molecular ions enveloped by much-extended partially-ionized hydrogen coronae that flow into space, a general structure shown schematically in Fig. 8.

We identify three requirements for Xe escape: (1) Xe atoms must become ionized and remain ionized. (2) The flow of H^+ to space must be great enough that collisions between the ions can push the Xe^+ ions upwards faster than they can be pulled back by gravity. (3) The Xe^+ ions must be transported by vertical winds through the cold lower

ionosphere where CO_2 is abundant to high enough altitudes that outflowing hydrogen can sweep them away. Here we discuss each requirement in turn.

Xenon is mostly ionized above the homopause. This occurs in part because Xe can be photo-ionized at wavelengths to which H_2 and H are transparent; in part because charge exchange of neutral Xe with CO_2^+ is fast; and in part because there is a dearth of recombination mechanisms faster than radiative recombination. In particular, Xe^+ does not react with H, H_2 or CO_2 . This partiality to life as an ion would change if O_2 were abundant, as was certainly the case after the GOE (Great Oxidation Event) ca 2.4–2.1 Ga (Catling and Kasting, 2017, p. 257), or if small hydrocarbons (other than CH_4) were abundant, as could have been the case if Archean Earth experienced a Titan-like pale orange dot phase (Domagal-Goldman et al., 2008; Arney et al., 2016). This is because O_2 and hydrocarbons like C_2H_2 charge exchange with Xe^+ (Anicich, 1993) to render Xe neutral and subject to falling back to Earth. If a Xe^+ ion reaches the hydrogen corona, it is very likely to remain ionized because of charge exchange with H^+ .

The H^+ escape flux depends on the hydrogen mixing ratio f_{H_2} and the flux of ionizing radiation S . In the Hadean, when S sometimes exceeded 40, and if everything else were favorable, Xe may have been able to escape with hydrogen mixing ratios as small as 0.4%. Otherwise more hydrogen is needed. The minimum f_{H_2} for Xe escape probably exceeded 1% in the Archean when S was smaller (the lower atmosphere could be 1% H_2 or 0.5% CH_4 to the same effect, because CH_4 is photochemically converted to H_2 and other products). The minimum EUV flux for Xe escape is in the range $10 < S < 15$, high enough that Xe escape would have been rare after 3.0 Ga. These specific properties of our model are likely to be shared by any model that uses hydrogen escape to drive Xe^+ into space. A more realistic model of the polar wind might drive off Xe with a smaller value of S , because other means of heating and ionizing would be available to a magnetically channeled polar wind.

Transport of Xe^+ through the cold molecular ionosphere (Fig. 8) is an unresolved issue. If the molecular ions themselves flow upwards with the hydrogen, then all is well with Xe^+ escape, but our model gives them no cause to do so. To describe vertical transport we introduced a third modeling parameter – an ion diffusivity K'_{zz} – to supplement the physical parameters S and f_{H_2} . By construction K'_{zz} acts only on ions, which are strongly coupled to each other by electromagnetic forces. Although fundamentally K'_{zz} is a modeling parameter, we can estimate its magnitude from observations of vertical winds in the thermosphere and by analogy to turbulent viscosity in astrophysical accretion disks. Both suggest that K'_{zz} could be of the order of $4 \times 10^9 \text{ cm}^2 \text{ s}^{-1}$. This is quite high compared to eddy diffusion amongst the neutrals, but we find that Xe cannot escape in our 1-D model if K'_{zz} is much smaller than $4 \times 10^8 \text{ cm}^2 \text{ s}^{-1}$. The dependence of Xe escape on K'_{zz} is more or less separate from the dependence on f_{H_2} ; the former affects transport through the lower ionosphere, whilst the latter affects transport in the escaping hydrogen corona. Thus our conclusions regarding the minimum amount of

hydrogen required in the atmosphere for Xe escape are not greatly affected by K'_{zz} .

5.1. Other omissions and future directions

We have omitted much in order to carve out a tractable problem. We have already mentioned transport through the molecular ions, which likely will require a 3-D MHD model to properly address. Three other important omissions are thermal conduction, O_2 , and O^+ ions.

Thermal conduction will smooth the thermal transition between the hydrogen corona and the molecular ionosphere, and it can slow hydrogen escape by transporting energy from the warm hydrogen corona to low altitudes where radiative cooling can be effective. Negligible differences between our results and those obtained using a time-dependent hydrocode that includes thermal conduction (Fig. 6) suggest that thermal conduction is not very important to hydrogen escape from Earth where $S > 2.5$. Our own numerical experiments with hydrostatic CO_2 - H_2 atmospheres suggest that hydrogen-rich atmospheres can be stabilized against escape by thermal conduction for $S < 1$. This should prove an interesting topic for further research.

Charge exchange with O_2 is a major threat to Xe^+ . The relatively oxidized CO_2 - H_2 atmospheres we have considered here are prone to spawning photochemical O_2 at high altitudes, especially given vigorous hydrogen escape. The O_2 threat can be mitigated by a generally more reduced atmosphere. Diluting CO_2 with CO or N_2 could go a long way toward reducing O_2 . O_2 could also be removed by a catalytic chemical cycle involving trace constituents, as apparently occurs on Venus. That Xe escape might require a more reduced atmosphere for early Earth than we have considered, perhaps leading to an upper bound on the amount of CO_2 in the Hadean or Archean, and the suggestion that Xe fractionation may have continued well into the Proterozoic in the face of O_2 (Warr et al., 2018), makes this an interesting direction to take further research.

Third, O^+ , if present, will escape if Xe^+ can escape. O^+ is a better carrier for Xe^+ escape than H^+ owing to its greater mass, it should be able to ionize Xe by charge exchange, and it is known to escape from Earth today (Shelley et al., 1972), although it is not known how (Shen et al., 2018). Considerable O^+ escape would imply less oxidation of Earth, but if the presence of O^+ were the signal of considerable amounts of O_2 (Mendillo et al., 2018), there would be few Xe^+ ions present and escape of Xe would be negligible. Because of this potential to undermine somewhat our conclusions on one hand, and the potential of helping Xe escape after the rise of oxygen on the other, we regard O^+ as calling for further research.

5.2. Conclusions

Our conclusion that the H_2 (or CH_4) atmospheric mixing ratio was at times at least 1% or higher through the Archean is important and perhaps unexpected. This conclusion is based on the minimum requirements for Xe to escape at any particular time and therefore appears to be

relatively robust. In particular, it is not greatly affected by the uncertainties attending the transport of Xe through the molecular ionosphere. Either H_2 or CH_4 would be important to early Earth because either gas would help create favorable environments for the origin of life (Urey, 1952; Tian et al., 2005). Both gases can provide greenhouse warming in the struggle against the faint young Sun (Wordsworth and Pierrehumbert, 2013).

What is not clear is how often the H_2 (or CH_4) atmospheric mixing ratio was 1% or higher. If much of the time, Earth could have lost more than an ocean's worth of hydrogen to space. This is comparable to the amount of oxygen stored in the mantle and crust as partner to Fe^{+3} and carbon, but it pushes hard against realistic upper bounds on how rapidly iron can be oxidized and cycled back into the mantle (Ozaki et al., 2018). The implication that Earth grew significantly more oxidized through the Archean may or may not be in conflict with evidence that the oxidation state of magma sources has changed (Aulbach et al., 2017) or not changed (Nicklas et al., 2018). However, the lost ocean is not a robust conclusion from our model, because the observed Xe fractionation can be generated by many different histories. In particular, histories that simultaneously account both for Xe's fractionation and its depletion require that Xe escape occurred in short intense bursts rather than as a constant trickle. Bursts of Xe escape can be caused by solar EUV variability, or by varying amounts of atmospheric hydrogen, or perhaps by changes in Earth's geomagnetic field. If hydrogen were less abundant ($< 0.1\%$) at most times, a lost ocean in the Archean becomes an order of magnitude overestimate.

In this paper we have presented Xe escape as an ion in the context of recent discoveries of evolving Xe preserved in ancient rocks spanning the Archean (Avice et al., 2018). Xenon escape in the Archean is a requirement that only escape as an ion can meet. Escape as an ion also explains how Xe escapes when Kr and Ar do not, which neatly resolves the paradox that has been the bane of traditional models of Xe fractionation in hydrodynamic escape. The mass fractionation mechanism itself is the same as in traditional hydrodynamic escape models: it is the competition between collisions and gravity, with the key difference being that the collisions that drive Xe^+ outward are between ions and governed by the Coulomb force.

Although we have not dwelt on the Hadean, the ion-escape model works very well on the ~ 200 Myr time scale of the early Hadean (or early Mars), when the Sun was a bigger source of EUV radiation. To make the ion-escape model work over the stretched out two billion year time-scale discovered by Avice et al. (2018) requires adding at least one other feature (limiting escape to narrow polar windows, or limiting Xe escape to brief episodes), or dropping the expectation that a single set of parameters should explain both Xe's fractionation and its depletion. If in fact Earth's Xe fractionation took place in the deep Hadean, such that the drawn out evolution of Xe isotopes documented by Avice et al. (2018) has other causes than the evolution of the atmosphere, the ion-escape model would still provide the best explanation of how Xe acquired its fractionation.

ACKNOWLEDGMENTS

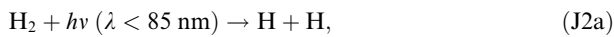
The authors thank JCG Walker, JF Kasting, T Donahue, R Kirshner, DM Hunten, JB Pollack, RO Pepin, G Wasserburg, M Ozima, B Marty, M Pujols, G Avicé, S Mukhopadhyay, A Hoffman, N Dauphas, JH Waite, and C Reinhard for specific advice and encouragement to quantify this hypothesis. DCC acknowledges support from Simons Foundation SCOL Award 511570, and NSF Frontiers in Earth System Dynamics award No. 1338810. KJZ and DCC acknowledge support from NASA Astrobiology Institute's Virtual Planetary Laboratory grant NNA13AA93A and Planetary Atmospheres grant NNX14AJ45G. MG was supported by a NASA NPP fellowship.

APPENDIX A. HYDROGEN ESCAPE FROM A CO₂-RICH ATMOSPHERE

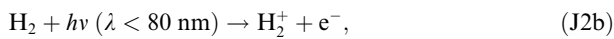
The goal here is to develop a description of hydrogen escape in the presence of a static background of CO₂ suitable for investigating Xe escape. Our equations are simplified from the self-consistent 5 moment approximation to multi-component hydrodynamic flow presented by (Schunk and Nagy, 1980). We merge this description with the description of two component diffusion given by Hunten (1973) to express collision terms in terms of binary diffusion coefficients and to include parameterized Eddy diffusivity in the lower atmosphere.

A.1. Chemistry

We begin with the photochemistry of the H₂-CO₂ atmosphere. We denote the three neutral species H, H₂, and CO₂ with the indices 1, 2, 3, respectively. H₂ is photolyzed by EUV radiation. It can be dissociated



ionized

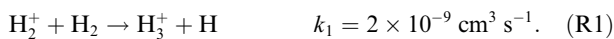


or dissociatively ionized

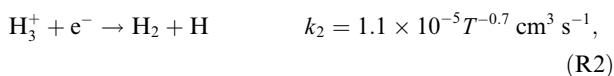


The relative yields of the three channels are, respectively, 0.56 : 0.35 : 0.09 for the solar EUV spectrum (Huebner et al., 1992). All channels eventually lead to dissociation of H₂, so that the total photodissociation rate is $J_2 = J_{2a} + J_{2b} + J_{2c}$.

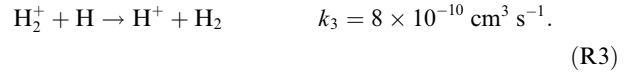
The H₂⁺ ion reacts quickly with any of the three major species. The reaction with H₂ forms the H₃⁺ ion, an important radiative coolant



The sink on H₃⁺ is dissociative recombination,



which, like dissociative recombination generally, is very fast. The reaction of H₂⁺ with H, a charge exchange, is a source of H⁺

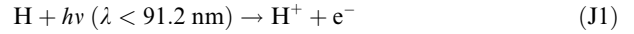


The reaction of H₂⁺ with CO₂ is also fast,

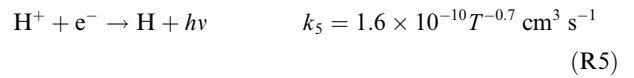


but the listed (McElroy et al., 2012) product, HCO₂⁺, appears likely to dissociatively recombine to form CO₂ and H, so that on net Reaction R4 does nothing to CO₂ while dissociating H₂.

Atomic H is photo-ionized by EUV radiation,



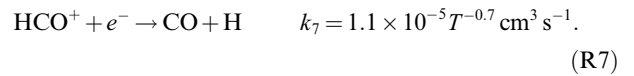
Radiative recombination of H⁺,



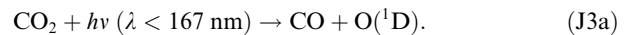
is about 5 orders of magnitude slower than dissociative recombination of H₃⁺, hence H⁺ is typically much more abundant than H₃⁺. At low altitudes the sink of H⁺ is a chemical reaction with CO₂



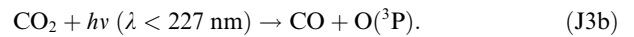
The formyl radical, HCO, is relatively easily ionized, and thus HCO⁺ is often abundant in astrophysical settings. We find it abundant in CO₂-H₂ atmospheres. The sink on HCO⁺ is dissociative recombination,



CO₂ can be photolyzed by both FUV and EUV. The most important FUV channel is dissociation to the excited O(¹D) state



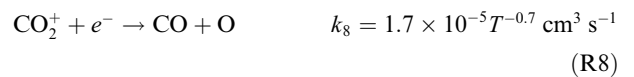
Although spin-forbidden, photo-dissociation to the ground state O(³P) does occur at a low rate. At 157 nm, the quantum yield of O(³P) is of the order of 0.1 (Schmidt et al., 2013). At wavelengths greater than 167 nm, where CO₂'s absorption cross-section is small but nonzero, we assume that the product is mostly O(³P),



Higher energy photons produce a variety of additional outcomes (Huebner et al., 1992), the most important of which is ionization,



The CO₂⁺ ion can dissociatively recombine



or it can react with H to form HCO⁺

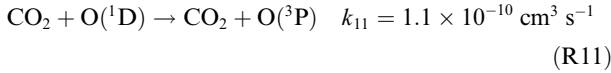


In this study we simplify the chemistry by omitting alternative paths that generate O^+ and O_2^+ from CO_2^+ . Oxygen ions in particular are interesting because they too will escape in any wind that can carry off Xe^+ . Because O^+ is more massive than H^+ , it is more efficient at driving off Xe^+ .

The $O(^1D)$ atoms produced by CO_2 photolysis react quickly with H_2 to form OH , which then reacts with CO to remake CO_2 . The reaction between $O(^1D)$ and H_2



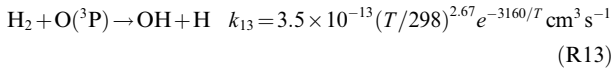
is very fast. The $O(^1D)$ can also be de-excited to the ground state by collisions with CO_2



or much less efficiently by collisions with atomic H (Krems et al., 2006)



The reaction between H_2 and $O(^3P)$



has a significant temperature barrier and is slow at room temperature. The reaction of CO and OH to reconstitute CO_2 is not particularly fast but lacks a significant activation barrier, which makes it by far the most important sink of CO



The reverse of R14 is endothermic and does not become fast until T approaches 2000 K. The net result of R10 (or R13) followed by R14 is reconstitution of CO_2 and dissociation of H_2 . Hence CO_2 tends to persist while H_2 persists, although as noted CO_2 is dissociated by ion chemistry. Here we will overlook dissociation of CO_2 and we will assume that reaction R13 is negligible. The net rate that CO_2 photolysis leads to dissociation of H_2 can then be written

$$CO_2 + hv + H_2 \rightarrow CO_2 + 2H \quad J'_3 \approx \frac{J_{3a} k_{10} n_2}{k_{12} n_1 + k_{10} n_2 + k_{11} n_3}, \quad (\text{R15})$$

which takes into account the sources and sinks of $O(^1D)$.

Ion chemistry

We solve for the five ions H^+ , H_2^+ , H_3^+ , CO_2^+ , and HCO^+ , which we denote as x_i , with i going from 1 to 5, respectively. Consistent with our neglecting O , CO , and O_2 , we neglect O^+ , O_2^+ , and OH^+ . We assume local photochemical equilibrium, which is a good approximation for the molecular ions, less good for H^+ at high altitudes where it is effectively the only ion. The equations are $\partial x_i / \partial t = 0$ for all i ; reaction rates are summarized in Table A.2.

$$\partial x_1 / \partial t = J_1 n_1 + J_{2c} n_2 + k_3 x_2 n_1 - k_5 x_1 n_e - k_6 x_1 n_3 \quad (\text{A.1})$$

$$\partial x_2 / \partial t = J_{2b} n_2 - k_1 x_2 n_2 - k_3 x_2 n_1 - k_4 x_2 n_3 \quad (\text{A.2})$$

$$\partial x_3 / \partial t = k_1 x_2 n_2 - k_2 x_3 n_e \quad (\text{A.3})$$

$$\partial x_4 / \partial t = J_{3c} n_3 - k_8 x_4 n_e - k_9 x_4 n_1 \quad (\text{A.4})$$

$$\partial x_5 / \partial t = k_6 x_1 n_3 - k_7 x_5 n_e + k_9 x_4 n_1 \quad (\text{A.5})$$

$$\sum x_i = n_e \quad (\text{A.6})$$

Dissociative recombination of H_2^+ is relatively slow; we omit it. Despite being very short-lived, the molecular ions (chiefly HCO^+) are dominant at low altitudes (as illustrated

Table A.2
Summary of H_2 - CO_2 Chemistry.

Label	Reactants	Products	Rate [$\text{cm}^3 \text{ s}^{-1}$]
J1	$H + hv$	$\rightarrow H^+ + e^-$	J_1
J2a	$H_2 + hv$	$\rightarrow H + H$	J_{2a}
J2b	$H_2 + hv$	$\rightarrow H_2^+ + e^-$	J_{2b}
J2c	$H_2 + hv$	$\rightarrow H + H^+ + e^-$	J_{2c}
J3a	$CO_2 + hv$	$\rightarrow CO + O(^1D)$	J_{3a}
J3b	$CO_2 + hv$	$\rightarrow CO + O(^3P)$	J_{3b}
J3c	$CO_2 + hv$	$\rightarrow CO_2^+ + e^-$	J_{3c}
R1	$H_2^+ + H_2$	$\rightarrow H_3^+ + H$	$k_1 = 2 \times 10^{-9}$
R2	$H_3^+ + e^-$	$\rightarrow H_2 + H$	$k_2 = 1.1 \times 10^{-5} T^{-0.7}$
R3	$H_2^+ + H$	$\rightarrow H_2 + H^+$	$k_3 = 8 \times 10^{-10}$
R4	$H_2^+ + CO_2$	$\rightarrow HCO_2^+ + H$	$k_4 = 2.4 \times 10^{-9}$
R5	$H^+ + e^-$	$\rightarrow H + hv$	$k_5 = 1.6 \times 10^{-10} T^{-0.7}$
R6	$H^+ + CO_2$	$\rightarrow HCO^+ + O$	$k_6 = 3.5 \times 10^{-9}$
R7	$HCO^+ + e^-$	$\rightarrow CO + H$	$k_7 = 1.1 \times 10^{-5} T^{-0.7}$
R8	$CO_2^+ + e^-$	$\rightarrow CO + O$	$k_8 = 1.7 \times 10^{-5} T^{-0.7}$
R9	$CO_2^+ + H$	$\rightarrow HCO^+ + O$	$k_9 = 2.9 \times 10^{-10}$
R10	$H_2 + O(^1D)$	$\rightarrow OH + H$	$k_{10} = 1.2 \times 10^{-10}$
R11	$CO_2 + O(^1D)$	$\rightarrow CO_2 + O(^3P)$	$k_{11} = 1.1 \times 10^{-10}$
R12	$H + O(^1D)$	$\rightarrow H + O(^3P)$	$k_{12} = 1 \times 10^{-12}$
R13	$H_2 + O(^3P)$	$\rightarrow OH + H$	$k_{13} = 3.5 \times 10^{-13} (T/298)^{2.67} e^{-3160/T}$
R14	$CO + OH$	$\rightarrow CO_2 + H$	$k_{14} = 1.5 \times 10^{-13}$

in Fig. 4 in the text). The important aspect of molecular ions in the present study is that they interact strongly with Xe^+ by the Coulomb force, and hence Xe^+ escape depends in part on transport by the molecular ions.

A.2. Radiative processes

We divide the EUV and FUV spectrum F_λ into sixteen wavelength bins that capture the essential colors for a $\text{CO}_2\text{-H}_2$ atmosphere. In particular, we bookkeep a channel between 80 nm and 91.2 nm for ionization of atomic hydrogen at wavelengths that do not ionize CO_2 or H_2 , and we account for CO_2 's anomalously low cross-section in the channel encompassing Lyman α .

A.2.1. Photolysis and optical depths

The total optical depth as a function of wavelength τ_λ is formally given by integration over the sum of the opacities of the different species

$$\partial\tau_\lambda/\partial r = \sum_i n_i \sigma_{i,\lambda} \quad (\text{A.7})$$

where $\sigma_{i,\lambda}$ is the cross section [cm^2] of species i at wavelength λ . Photolysis rates and photoionization rates J_i are obtained as integrals of the form

$$J_i = S \int F_\lambda \sigma_{i,\lambda} \exp(-\tau_\lambda) d\lambda. \quad (\text{A.8})$$

where F_λ refers to the modern mean solar XUV spectrum and S refers to the enhanced ancient solar XUV flux relative to the modern Sun (Eq. (2) of the main text). The units of J_i are s^{-1} .

A.2.2. Radiative heating

The local radiative volume heating rate [$\text{ergs cm}^{-3} \text{s}^{-1}$] is given by

$$\Gamma_h = S \eta_h \sum_i n_i \sigma_{i,\lambda} \frac{F_\lambda hc}{\lambda} \exp(-\tau_\lambda) \quad (\text{A.9})$$

where h is Planck's constant and c is the speed of light, and $\eta_h \approx 0.5$ is a heating efficiency (Koskinen et al., 2014).

The total radiative heating, the integral of Γ_h , can be used to define an energy-limited flux. The energy-limited flux is intended to be an upper bound that compares the energy incident in XUV radiation to the energy required to lift the atmosphere into space (Watson et al., 1981). Details are lumped together in a different efficiency factor $\eta \neq \eta_h$ that is often taken to lie between 0.1 and 0.6 (Lammer et al., 2013; Bolmont et al., 2017). The energy-limited flux can be expressed either in terms of F_{xuv} , or in terms of the total solar radiation absorbed above some arbitrary altitude, a definition that implicitly takes FUV into account. With FUV taken into account, η can exceed unity.

We consider two forms of the energy-limited fluxes of H_2 molecules [$\text{cm}^{-2} \text{s}^{-1}$],

$$\phi_{\text{EL}} = \frac{S \eta hc R_\oplus}{4GM_\oplus m_2} \int_0^{91.2 \text{ nm}} \int_0^\infty \lambda^{-1} F_\lambda \exp(-\tau_\lambda) d\lambda d\tau_\lambda, \quad (\text{A.10})$$

where all the photons with $\lambda < 91.2$ nm are absorbed, and

$$\phi'_{\text{EL}} = \frac{S \eta hc R_\oplus}{4GM_\oplus m_2} \int_0^{200 \text{ nm}} \int_0^{\tau_\lambda(r_0)} \lambda^{-1} F_\lambda \exp(-\tau_\lambda) d\lambda d\tau_\lambda, \quad (\text{A.11})$$

where $\tau_\lambda(r_0)$ represents the optical depths at the lower boundary. In Eqs. (A.10) and (A.11), M_\oplus and R_\oplus refer to the mass and radius of Earth; m_2 is the mass of an H_2 molecule; hc/λ is the energy of a photon [ergs]; and τ_λ is the optical depth as a function of λ . Eqs. (A.10) and (A.11) are evaluated with $\eta = 0.5$ to compare to the fluxes computed with the full model in Figs. 5 and 6 of the main text.

A.2.3. CO_2 cooling

The major coolant of the thermospheres of Earth, Venus and Mars is collisional excitation of the v_2 vibrational band of CO_2 , probably by atomic oxygen, followed by emission of a 15 micron photon. We use the relatively simple algorithm described by Gordiets et al. (1982), based on work by James and Kumer (1973) and Kumer and James (1974), which prioritizes generality over fidelity. We have had to make some notational changes to avoid potential confusion with other symbols used in this study; the correspondences to the original notation are given in the Table of Symbols (Appendix C). The volume cooling rate [$\text{ergs cm}^{-3} \text{s}^{-1}$] is

$$\Gamma_{\text{CO}_2} = 2h\nu_2 n_{\text{CO}_2} \times \sum_j k_j^* n_j \times \Theta(\Lambda, \tau) \exp(-960/T) \quad (\text{A.12})$$

where $h\nu_2 = 1.33 \times 10^{-13}$ ergs. The collisional excitation and de-excitation rate is summed over all the constituents present, $\sum_j k_j^* n_j$. Atomic oxygen is usually regarded as dominant for Venus, Earth, and Mars, with a collisional excitation rate k_o^* on the order of $2 \times 10^{-12} \text{ cm}^3 \text{s}^{-1}$, but factor two mismatches between what the models require and what is observed in the laboratory remain unresolved (Sharma and Wintersteiner, 1990; Bougher et al., 1994; Sharma, 2015). For a hydrogen-rich atmosphere, excitation will be dominated by H_2 and H. The rate for $k_{\text{H}_2}^*$ is known to be rather high, $5 \times 10^{-12} \text{ cm}^3 \text{s}^{-1}$ at 300 K and $7.5 \times 10^{-12} \text{ cm}^3 \text{s}^{-1}$ at 200 K (Allen et al., 1980; Sharma, 2015); we use the lower of these. We presume $k_{\text{H}}^* = 1 \times 10^{-11} \text{ cm}^3 \text{s}^{-1}$, a rate consistent with the thermodynamic reverse of $\text{R14 CO} + \text{OH}$. Excitation by CO_2 itself is negligible by comparison; we use $k_{\text{CO}_2}^* = 2 \times 10^{-14} \text{ cm}^3 \text{s}^{-1}$.

The parameter τ_x is a line center optical depth.

$$\tau_x = \sigma_{v_2} n_3 H_3, \quad (\text{A.13})$$

where $\sigma_{v_2} = 6.4 \times 10^{-15} \text{ cm}^2$ is an effective absorption cross section at the center of the v_2 band. The parameter Λ describes the competition between radiative and collisional de-excitation,

$$\Lambda = \frac{A_{v_2}}{A_{v_2} + \sum_j k_j^* n_j}. \quad (\text{A.14})$$

The spontaneous emission rate is $A_{v_2} = 1.35 \text{ s}^{-1}$. The function $\Theta(\Lambda, \tau_x)$ is the normalized chance that a photon escapes

$$\Theta(\Lambda, \tau_x) = \frac{(E(\tau_x) + E(0.5\tau_x))\Lambda}{2 - 2\Lambda + (E(\tau_x) + E(0.5\tau_x))\Lambda} \quad (\text{A.15})$$

where we have used a curve fit to the tabulated values of an exponential function $E(\tau_x)$ (Doppler broadening) in [Kumer and James \(1974\)](#) that [Gordiets et al. \(1982\)](#) refer to,

$$E(\tau_x) \approx \frac{8.54}{17.15 + \tau_x^{1.08}} + \frac{0.272}{141.7 + \tau_x^{0.53}} \quad (\text{A.16})$$

The 4.3 micron v_3 band is stronger than the 15 micron v_2 band, but usually less important for cooling because the temperature must be higher to excite it. We use the same formalism as Eq. (A.12) with parameters appropriate to the v_3 band: $h\nu_3 = 4.5 \times 10^{-13}$ ergs, $\sigma_{v_3} = 2.47 \times 10^{-14} \text{ cm}^2$, and $A_{v_3} = 400 \text{ s}^{-1}$. The excitation temperature is 3350 K. Because the A value is higher, the 4.3 μm band is less easily collisionally quenched, and hence it can effectively cool from deeper levels in the atmosphere than the 15 μm band.

A.2.4. H_3^+ cooling

The molecular ion H_3^+ is known to be an effective coolant. It is important in the energy budgets of the solar system's giant planets, and [Yelle \(2004\)](#) showed it to be a major part of the budget of highly irradiated exo-Jupiters. It is reasonable to expect it be important for mildly irradiated H_2 -rich ionospheres we are considering here. We use a curve fit to cooling rates computed by [Neale et al. \(1996\)](#) to obtain the volume cooling rate

$$\Gamma_{\text{H}_3^+} = 4\pi x_3 \exp\left(-a_1 + a_2 \ln(T) - a_3 (\ln(T))^2\right) \quad (\text{A.17})$$

where $a_1 = 118.85$, $a_2 = 21.488$, and $a_3 = 1.2308$. The fit is for $500 < T < 3500$, which covers the range of interest for the present application.

A.2.5. Cooling by H and H^+

Cooling by H and H^+ can be important in the high altitude atomic ionosphere. The volume cooling rate for free-free cooling is

$$\Gamma_{ff} \approx 1.7 \times 10^{-27} x_1 n_e T^{1/2} \text{ ergs cm}^{-3} \text{ s}^{-1} \quad (\text{A.18})$$

and for bound-free cooling is

$$\Gamma_{bf} \approx 2.5 \times 10^{-25} x_1 n_e \text{ ergs cm}^{-3} \text{ s}^{-1}. \quad (\text{A.19})$$

These turn out never to be important. Collisional excitation of Ly α is very important at temperatures on the order of $\sim 1 \times 10^4$ K ([Murray-Clay et al., 2009](#)), but is negligible for $T < 8000$ K. We will not encounter conditions where Lyman α cooling is important in this study.

A.2.6. Radiative effects of neglected species

We have omitted N_2 , NO, CO, O, OH, H_2O , and O_2 . Although N_2 itself does not radiate unless very hot, the lowest vibrationally excited states of N_2 are resonant with the v_3 CO_2 asymmetric stretch at 4.3 μm , and thus collisional excitation of N_2 leads directly to 4.3 μm CO_2 radiation (the mechanism behind CO_2 lasers). This can be important

where N_2 is more abundant than CO_2 and the gas is warm. Atomic oxygen and nitric oxide are important radiative coolants on Earth today ([Kulikov et al., 2007](#)), and would likely be important on early Earth as well. The 4.8 μm CO band can be an effective coolant if the atmosphere is hot. Rotational cooling by CO is important at low temperatures and low densities in astrophysical settings. Water will be present at ~ 100 ppm while H_2 persists, produced by $\text{H}_2 + \text{OH} \rightarrow \text{H}_2\text{O} + \text{H}$ and destroyed by $\text{H}_2\text{O} + h\nu \rightarrow \text{OH} + \text{H}$. Water emission at 6.3 μm can be an effective coolant, but water is also a much stronger FUV absorber than CO_2 ; exploratory numerical experiments suggest that heating is probably more important than cooling. Molecular oxygen is a poor radiative coolant but a strong FUV absorber; its role is unambiguously to heat.

A.3. Vertical structure equations

We make several sweeping simplifications to the basic equations given by [Schunk and Nagy \(1980\)](#). As we are considering a relatively dense gas, we use a single temperature T for all species. We also assume steady state and spherical symmetry. Densities, masses, and velocities of neutral species i are denoted n_i , m_i , and v_i , respectively.

A.3.1. Continuity

Conservation of species i can be written

$$\frac{1}{r^2} \frac{\partial(r^2 n_i v_i)}{\partial r} = P_i - L_i \quad (\text{A.20})$$

where P_i and L_i are photochemical production and loss terms. For hydrogen, we include only two terms: direct photolysis of H_2 , and the splitting of H_2 that takes place when $\text{O}(\text{D})$ from CO_2 photolysis reacts with H_2 .

$$\frac{1}{r^2} \frac{\partial(r^2 v_1 n_1)}{\partial r} = 2J_2 n_2 + 2J'_3 n_3 \quad (\text{A.21})$$

$$\frac{1}{r^2} \frac{\partial(r^2 v_2 n_2)}{\partial r} = -J_2 n_2 - J'_3 n_3 \quad (\text{A.22})$$

All the equations are greatly simplified if we assume that both H and H_2 flow upwards with the same velocity $v_1 = v_2 = u$. With this useful simplification, total hydrogen conservation reduces to

$$\frac{1}{r^2} \frac{\partial(r^2 u (0.5n_1 + n_2))}{\partial r} = 0. \quad (\text{A.23})$$

The integral of Eq. (A.23) is the constant

$$r_0^2 \phi_{\text{H}_2} = (0.5n_1 + n_2) u r^2, \quad (\text{A.24})$$

where we have defined ϕ_{H_2} as the total hydrogen escape flux as measured at the lower boundary.

When hydrogen is the only element escaping, it is useful to define a total hydrogen number density $n' = n_1 + n_2$ and a mean molecular weight for hydrogen,

$$\mu' = \frac{n_1 m_1 + n_2 m_2}{n'}. \quad (\text{A.25})$$

The prime denotes that μ' refers only to the hydrogen and not to the whole atmosphere. Eqs. (A.21) and (A.22) are summed for the change in n'

$$\frac{1}{r^2} \frac{\partial(r^2 u n')}{\partial r} = J_2 n_2 + J_3 n_3. \quad (\text{A.26})$$

The mean molecular weight μ' of the hydrogen varies in response to photolysis,

$$\frac{1}{\mu'} \frac{\partial \mu'}{\partial r} = -\frac{J_2 n_2 + J_3 n_3}{(n_1 + n_2) u}. \quad (\text{A.27})$$

We will use Eq. (A.27) to develop a planetary wind equation.

A.3.2. Conservation of momentum

Starting from Schunk and Nagy (1980), and after many simplifying assumptions, momentum conservation in spherical symmetry for a constituent i in the presence of other constituents j can be written

$$n_i m_i v_i \frac{\partial v_i}{\partial r} + \frac{\partial(n_i k_B T)}{\partial r} = -\frac{GM_{\oplus} n_i m_i}{r^2} - \sum_j (v_i - v_j) n_i n_j \frac{k_B T}{b_{ij}}. \quad (\text{A.28})$$

The collision terms are appropriate to the 5-moment approximation in the limit that all the species have the same temperature; according to Schunk and Nagy (1980) these collision terms are valid for the Maxwell interaction potential (inverse fourth power) for arbitrary relative velocities, which provides some justification for using them in cases where $v_i - v_j$ might approach the sound speed. The mapping between the momentum transfer collision frequencies v_{ij} used by Schunk and Nagy (1980) and the binary diffusion coefficients used by Hunten (1973) is

$$v_{ij} = \frac{k_B T}{m_i} \frac{n_j}{b_{ij}}. \quad (\text{A.29})$$

Unlike v_{ij} , the binary diffusion coefficient is symmetrical, $b_{ij} = b_{ji}$.

Eddy mixing in the lower atmosphere – absent from Eq. (A.28) – is introduced following Hunten (1973), who implicitly defines the eddy diffusion coefficient K_{zz} in terms of a total number density $n = \sum_i n_i$ and an appropriate average value \bar{b} of b_{ij} .

$$\frac{m_i v_i}{k_B T} \frac{\partial v_i}{\partial r} + \frac{1}{n_i} \frac{\partial n_i}{\partial r} + \frac{1}{T} \frac{\partial T}{\partial r} = -\frac{GM_{\oplus} m_i}{r^2 k_B T} - \sum_j \frac{(v_i - v_j) n_j}{b_{ij}} - \frac{K_{zz} n}{\bar{b}} \left(\frac{1}{n_i} \frac{\partial n_i}{\partial r} - \frac{1}{n} \frac{\partial n}{\partial r} \right). \quad (\text{A.30})$$

Eq. (A.30) converges on the correct limiting expression for the bulk atmosphere's hydrostatic scale height when summed over the many constituents in the limit that the u^2 terms can be ignored,

$$\frac{1}{n} \frac{\partial n}{\partial r} = -\frac{1}{T} \frac{\partial T}{\partial r} - \frac{GM_{\oplus} \mu}{r^2 k_B T}. \quad (\text{A.31})$$

The most important binary diffusion coefficient in the CO₂-H₂ system is (not surprisingly) b_{23} between CO₂ and H₂:

$$b_{23} = 31.4 \frac{T^{0.75} \exp(-11.7/T)}{k_B} \approx 1.2 \times 10^{19} (T/200\text{K})^{0.75} \text{ cm}^{-1} \text{ s}^{-1}. \quad (\text{A.32})$$

We will take $\bar{b} = b_{23}$. A homopause density n_h can be defined by $n_h \equiv K_{zz}/\bar{b}$.

The forces on hydrogen

Here we wish to construct an expression that describes hydrogen escape. First, we expand Eq. (A.30) into two equations, one for H ($i = 1$) and the other for H₂ ($i = 2$). We next impose the approximation that H and H₂ flow as a single fluid with velocity u . With $v_1 = v_2 = u$ as an additional constraint, neither Eq. (A.30) for H ($i = 1$) nor Eq. (A.30) for H₂ ($i = 2$) hold individually. The mass-weighted sum of the two Eqs. (A.30) for H and H₂ remains valid because the b_{12} terms that couple H and H₂ cancel out. This sum is written

$$\frac{n_1 m_1 + n_2 m_2}{k_B T} \frac{u \partial u}{\partial r} + \frac{\partial n'}{\partial r} + \frac{n'}{T} \frac{\partial T}{\partial r} = -\frac{GM}{r^2} \frac{n_1 m_1 + n_2 m_2}{k_B T} - \frac{K_{zz} n}{\bar{b}} \frac{\partial n'}{\partial r} + \frac{K_{zz} n}{\bar{b}} \frac{n'}{n} \frac{\partial n}{\partial r} - u n_3 \left(\frac{n_1}{b_{13}} + \frac{n_2}{b_{23}} \right). \quad (\text{A.33})$$

Subsequent derivations are clearer in terms of μ' and the hydrogen density $\rho' \equiv n' \mu'$

$$\frac{\rho'}{k_B T} \frac{u \partial u}{\partial r} + \frac{\partial(\rho'/\mu')}{\partial r} + \frac{\rho'}{\mu' T} \frac{\partial T}{\partial r} = -\frac{GM}{r^2} \frac{\rho'}{k_B T} - \frac{K_{zz} n}{\bar{b}} \frac{\partial(\rho'/\mu')}{\partial r} + \frac{\rho'}{\mu'} \frac{K_{zz} n}{\bar{b}} \frac{1}{n} \frac{\partial n}{\partial r} - u n_3 \left(\frac{n_1}{b_{13}} + \frac{n_2}{b_{23}} \right). \quad (\text{A.34})$$

Using Eq. (A.31) and gathering terms, Eq. (A.34) can be rewritten

$$\frac{\rho'}{k_B T} \frac{u \partial u}{\partial r} + \left(1 + \frac{K_{zz} n}{\bar{b}} \right) \left(\frac{1}{\rho'} \frac{\partial \rho'}{\partial r} + \frac{1}{T} \frac{\partial T}{\partial r} - \frac{1}{\mu'} \frac{\partial \mu'}{\partial r} \right) = -\frac{GM}{r^2 k_B T} \left(\mu' + \frac{K_{zz} n \mu'}{\bar{b}} \right) - \frac{u n_3}{n_1 + n_2} \left(\frac{n_1}{b_{13}} + \frac{n_2}{b_{23}} \right). \quad (\text{A.35})$$

Substituting for ρ' from continuity Eq. (A.26)

$$\frac{1}{\rho'} \frac{\partial \rho'}{\partial r} = \frac{1}{u} \frac{\partial u}{\partial r} - \frac{2}{r}, \quad (\text{A.36})$$

and using Eq. (A.27) to replace $\partial \mu'/\partial r$, results in an equation for the velocity gradient $\partial u/\partial r$ that resembles the usual solar wind equation,

$$(u^2 - c^2) \frac{1}{u} \frac{\partial u}{\partial r} = -\frac{GM_{\oplus}}{r^2} \left(1 + \frac{K_{zz} n}{b_{23}} \frac{\mu}{\mu'} \right) + \frac{2c^2}{r} - \frac{c^2}{T} \frac{\partial T}{\partial r} - \frac{n_3 u k_B T}{m_2 b_{23}} - \frac{c^2}{u} \times \frac{J_2 n_2 + J_3 n_3}{n_1 + n_2} \quad (\text{A.37})$$

where the quantity

$$c'^2 \equiv \frac{k_B T}{\mu'} \left(1 + \frac{K_{zz} n}{b_{23}} \right) \quad (\text{A.38})$$

takes on the role of the sound speed (squared). There are some advantages to solving Eq. (A.37) for $u(r)$ rather than solving for $n_1(r)$ and $n_2(r)$ directly. First, there is only one variable. Second, the singularity (the critical point) in the system at $u = c'$ is explicit. Often one solves an equation like Eq. (A.37) by solving for the critical point's location, then evaluating the gradient $\partial u / \partial r$ using L'Hôpital's rule, then numerically integrating downward to the lower boundary. The critical point conditions are iterated until the desired lower boundary conditions are met. This works well for simpler systems but becomes cumbersome for an equation like Eq. (A.37) for which the L'Hôpital's rule expression for $\partial u / \partial r$ at the critical point is complicated. Here we will integrate Eq. (A.37) for $u(r)$ upward from the lower boundary and iterate until the desired outer boundary conditions are closely approached.

Atomic and molecular hydrogen densities are obtained from Eq. (A.37) and continuity

$$\frac{1}{n_2} \frac{\partial n_2}{\partial r} = -\frac{1}{u} \frac{\partial u}{\partial r} - \frac{2}{r} - \frac{J_2 n_2 + J_3' n_3}{n_2 u}. \quad (\text{A.39})$$

and

$$\frac{1}{n_1} \frac{\partial n_1}{\partial r} = -\frac{1}{u} \frac{\partial u}{\partial r} - \frac{2}{r} + \frac{2J_2 n_2 + 2J_3' n_3}{n_2 u}. \quad (\text{A.40})$$

The forces on carbon dioxide

In this study, carbon dioxide is hydrostatic ($v_3 = 0$) and does not dissociate. Using Eq. (A.31) to describe mixing with the lower atmosphere, Eq. (A.30) with $j = 3$ reduces to

$$\begin{aligned} & \left(1 + \frac{K_{zz} n}{b} \right) \left(\frac{1}{n_3} \frac{\partial n_3}{\partial r} + \frac{1}{T} \frac{\partial T}{\partial r} \right) \\ &= -\frac{GM_{\oplus}}{r^2 k_B T} \left(m_3 + \frac{K_{zz} n \mu}{b} \right) + u \left(\frac{n_1}{b_{13}} + \frac{n_2}{b_{23}} \right). \end{aligned} \quad (\text{A.41})$$

We then simplify Eq. (A.41) by approximating $b_{13} = 2b_{23}$ and expressing u in terms of the total hydrogen flux

$$\begin{aligned} & \left(1 + \frac{K_{zz} n}{b_{23}} \right) \left(\frac{1}{n_3} \frac{\partial n_3}{\partial r} + \frac{1}{T} \frac{\partial T}{\partial r} \right) \\ &= -\frac{GM_{\oplus}}{r^2 k_B T} \left(m_3 + \frac{K_{zz} n \mu}{b_{23}} \right) + \frac{\phi_{H_2} r_0^2}{b_{23} r^2} \end{aligned} \quad (\text{A.42})$$

Eq. (A.42) is used to integrate $n_3(r)$ from the lower boundary.

The diffusion-limited flux – the upper bound on how fast hydrogen can diffuse through a hydrostatic atmosphere of CO_2 – can be recovered from Eq. (A.42) in the limit of constant mixing ratios (Zahnle and Kasting, 1986; Hunten et al., 1987). The K_{zz} terms drop out. In the particular case of H_2 diffusing through CO_2 , the diffusion limit is

$$\phi_{\text{DL}} = \frac{(m_3 - m_2) GM_{\oplus} b_{23} f_{H_2}}{r_0^2 k T}, \quad (\text{A.43})$$

where b_{23} is the binary diffusion coefficient between H_2 and CO_2 . For Earth, Eq. (A.43) evaluates to

$$\phi_{\text{DL}} = 3.0 \times 10^{13} f_{H_2} \left(\frac{200}{T} \right)^{0.25} \text{ cm}^{-2} \text{ s}^{-1}. \quad (\text{A.44})$$

Eq. (A.44) is used in Fig. 5. Important points about diffusion-limited escape are (i) it is proportional to the hydrogen mixing ratio and (ii) it remains valid as an upper limit on how quickly two species can be separated, even if both species escape.

A.3.3. Conservation of energy

Energy equations can be written for each species in steady state and spherical symmetry (Schunk and Nagy, 1980).

$$\begin{aligned} & \frac{3v_i}{2} \frac{\partial(n_i k_B T_i)}{\partial r} + \frac{5n_i k_B T_i}{2} \frac{1}{r^2} \frac{\partial(r^2 v_i)}{\partial r} + \frac{1}{r^2} \frac{\partial(r^2 Q_i)}{\partial r} \\ &= \Gamma_i + \sum_j \frac{n_i m_i v_{ij}}{m_i + m_j} \left(3k_B (T_j - T_i) + m_j (v_i - v_j)^2 \right) \end{aligned} \quad (\text{A.45})$$

where Γ_i represents the diabatic volume heating and cooling rates. The collision terms between the species are written out. Eq. (A.45) as written applies to monatomic species.

The simplest approximation to Eq. (A.45) assumes that all species share the same temperature. We then treat the fluid as a whole for the purposes of energy conservation,

$$\begin{aligned} & \frac{1}{r^2} \frac{\partial}{\partial r} \left\{ r^2 \sum_i n_i v_i m_i \left(\frac{v_i^2}{2} + \frac{\gamma_i}{\gamma_i - 1} \frac{k_B T}{m_i} - \frac{GM_{\oplus}}{r} \right) + r^2 \sum_i Q_i \right\} \\ &= \Gamma_h - \Gamma_c \end{aligned} \quad (\text{A.46})$$

where γ_i is the ratio of heat capacities of species i ($\gamma = 5/3$ for a monatomic gas); $Q = \sum_i Q_i$ represents the thermal conduction flux; and Γ_h and Γ_c refer to total radiative volume heating and cooling rates, respectively. Written in this form with $T_i = T$ for all i , the collisional terms in Eq. (A.45) either zero out or cancel out.

In general, thermal conduction is a complicated transport phenomenon, a proper treatment of which far exceeds the scope of this paper. We will estimate the magnitude of the term using the familiar approximation

$$Q = -k_c \frac{\partial T}{\partial r}, \quad (\text{A.47})$$

which is written in terms of a thermal conductivity k_c (k_c is a function of composition and temperature). In passing we note that thermal conduction as approximated by Eq. (A.47) implicitly assumes instantaneous transport of energy, when in fact energy transport by thermal conduction is bounded by the speed of sound, which is an important consideration for energy transport in a transonic planetary wind.

As above, we assume that H and H_2 flow outward with the same velocity u , and that CO_2 is hydrostatic. The usual diatomic $\gamma = 7/5$ for H_2 is assumed,

$$\begin{aligned} & \frac{1}{r^2} \frac{\partial}{\partial r} \left\{ r^2 n_1 u m_1 \left(\frac{u^2}{2} + \frac{5}{2} \frac{k_B T}{m_1} - \frac{GM_{\oplus}}{r} \right) \right. \\ & \quad \left. + r^2 n_2 u m_2 \left(\frac{u^2}{2} + \frac{7}{2} \frac{k_B T}{m_2} - \frac{GM_{\oplus}}{r} \right) \right\} \\ & + \frac{1}{r^2} \frac{\partial(r^2 Q)}{\partial r} = \Gamma_h - \Gamma_c. \end{aligned} \quad (\text{A.48})$$

The left hand side of Eq. (A.48) describes the divergence of advected kinetic energy and heat, work done lifting the gas out of the planet's potential well, and thermal conduction. These are equated to the sum of radiative heating and cooling.

Expanded with substitutions, Eq. (A.48) becomes

$$\begin{aligned} & \frac{\phi_{\text{H}_2} r_0^2}{r^2} \left\{ m_2 \left(\frac{GM_{\oplus}}{r^2} + u \frac{\partial u}{\partial r} \right) + \frac{7k_B}{2} \frac{\partial T}{\partial r} \right\} \\ & + \frac{3k_B T}{2} (J_2 n_2 + J'_3 n_3) + \frac{3k_B n_1 u}{4} \frac{\partial T}{\partial r} \\ & + \frac{1}{r^2} \frac{\partial(r^2 Q)}{\partial r} = \Gamma_h - \Gamma_c. \end{aligned} \quad (\text{A.49})$$

The terms involving J_2 and $n_1 u$ arise because photolysis increases the heat capacity of the gas by increasing the total number. Eq. (A.49) can be recast as an expression for the temperature gradient,

$$\begin{aligned} & \left(\frac{7k_B}{2} \phi_{\text{H}_2} + n_1 u \frac{3k_B}{4} n_1 u \right) \frac{\partial T}{\partial r} \\ & = \frac{r^2}{r_0^2} (\Gamma_h - \Gamma_c) - m_2 \phi_{\text{H}_2} \frac{GM_{\oplus}}{r^2} - m_2 \phi_{\text{H}_2} \frac{u \partial u}{\partial r} \\ & - \frac{r^2}{r_0^2} \frac{3k_B T}{2} (J_2 n_2 + J'_3 n_3) - \frac{1}{r_0^2} \frac{\partial(r^2 Q)}{\partial r}. \end{aligned} \quad (\text{A.50})$$

At this point we make two additional simplifications to enhance numerical stability. First, we drop the u^2 kinetic energy terms as small compared to the advected heat terms. This approximation eliminates a sometimes numerically troublesome term at little cost to the overall verisimilitude of the model. Second, we drop thermal conduction Q . With these approximations, Eq. (A.50) reduces to

$$\frac{\partial T}{\partial r} = \frac{\frac{r^2}{r_0^2} (\Gamma_h - \Gamma_c) - m_2 \phi_{\text{H}_2} \frac{GM_{\oplus}}{r^2} - \frac{r^2}{r_0^2} \frac{3k_B T}{2} (J_2 n_2 + J'_3 n_3)}{\frac{7k_B}{2} \phi_{\text{H}_2} + \frac{3k_B}{4} n_1 u}. \quad (\text{A.51})$$

Thermal conduction is important when the insolation is modest and the escape flux is small or negligible, especially in cases where a hydrostatic atmosphere can be stabilized by thermal conduction (Gross, 1972). For Earth and N₂-CO₂-H₂ atmospheres, hydrostatic solutions of this kind are possible for $S < 1$. But for a highly-irradiated planet like young Earth, ignoring Q is an acceptable shortcut, because thermal conduction cannot simultaneously be a big term in the energetics yet also span the dimensions of a much inflated thermosphere. In particular, we do not expect thermal conduction to much exceed a 10% effect for $S > 10$, which we will find to be the minimum S required for Xe escape. Fig. 6, which compares our results for hydrogen escape to those obtained using a hydrocode that includes thermal conduction (Kuramoto et al., 2013), implies that thermal conduction can be neglected for $S > 2.5$ with no obvious consequences. However, we do compute Q from our solutions as an *a posteriori* check for self-consistency.

A.4. Method of solution

The system is solved with the shooting method, integrating upward starting from below the homopause.

The basic equations are Eq. (A.37) for $u(r)$, Eqs. (A.39) and (A.40) for $n_1(r)$ and $n_2(r)$, Eq. (A.42) for $n_3(r)$, and Eq. (A.51) for $T(r)$. We seek a transonic solution that has just enough energy at the critical point to escape. The second outer boundary condition is in keeping with the philosophy that nothing that happens beyond the critical point can influence the atmosphere at the lower boundary.

We assume a density $n(r_0)$, eddy diffusivity K_{zz} , and total hydrogen escape flux ϕ_{H_2} at the lower boundary. The temperature $T(r_0)$ is determined by solving the local energy balance between absorbed XUV and FUV radiation and radiative cooling by CO₂, with the temperature gradient $(dT/dr)_0 = 0$. The nominal values of $n(r_0)$ and K_{zz} are $1 \times 10^{13} \text{ cm}^{-3}$ and $2 \times 10^6 \text{ cm}^2 \text{ s}^{-1}$, respectively. The lower boundary density is larger than the nominal homopause density $n_h \equiv b_{23}/K_{zz} = 6 \times 10^{12} \text{ cm}^{-3}$ in our nominal model.

The total H₂ mixing ratio at the lower boundary and the total hydrogen flux ϕ_{H_2} are treated as independent free parameters. We then solve for the solar irradiation S required to support ϕ_{H_2} . The irradiation S is iterated until the hydrogen velocity u matches the speed of sound at the point where the specific energy of the wind e_s ,

$$\begin{aligned} e_s = & f_{\text{H}_2} \left(\frac{7k_B T}{2} + m_{\text{H}_2} \left(\frac{u^2}{2} - \frac{GM_{\oplus}}{r} \right) \right) \\ & + f_{\text{H}} \left(\frac{5k_B T}{2} + m_{\text{H}} \left(\frac{u^2}{2} - \frac{GM_{\oplus}}{r} \right) \right) \end{aligned} \quad (\text{A.52})$$

is just sufficient to ensure escape with no further energy input. The second outer boundary condition is therefore

$$e_s(r_c) = \frac{2GM_{\oplus}}{r_c}. \quad (\text{A.53})$$

Eq. (A.52) omits CO₂ as negligible at r_c , and it neglects the chemical energy that would be released if the hydrogen were to recombine.

Optical depths and the quantities that depend on them – radiative heating, radiative cooling, and photolysis – are problematic for the shooting method because they should be computed by integrating inward from infinity. This is inconvenient when shooting outward from deep within the atmosphere. However, because optical depth appears only as an integrated quantity, none of the computations in this study critically depend on an exact value of τ . All that is really required are plausible values that decrease monotonically as the shooting algorithm ascends. Hence we make a local approximation to optical depth at each height using local densities and the local scale height,

$$\tau_{i\lambda} \approx n_i \sigma_{i\lambda} H \quad (\text{A.54})$$

$$H = k_B T / \mu g \quad (\text{A.55})$$

$$\tau_{i\lambda} \approx \sigma_{i\lambda} H n_i \quad (\text{A.56})$$

where μ is the mean molecular mass averaged over the different constituents. Comparison between our results for hydrogen escape and those obtained with a hydrocode that self-consistently computes optical depths (Fig. 6, Kuramoto et al., 2013) shows no sign that our local approximation to τ is failing in any important way.

A.5. Results for hydrogen escape

It is helpful to illustrate the properties of a particular model in some detail. For this purpose we have chosen a model (hereafter referred to as the “nominal” model) for illustration that lies well within the field of models for which Xe escape is predicted to take place. The key parameters are a relatively high EUV flux ($S = 20$) and a relatively high hydrogen mixing ratio ($f_{\text{H}_2} = 0.03$). Other nominal parameters are $n(r_0) = 1 \times 10^{13} \text{ cm}^{-3}$, $K_{zz} = 2 \times 10^6 \text{ cm}^2 \text{ s}^{-1}$, and spherical symmetry. Our models of hydrogen escape are not very sensitive to the latter three parameters. The computed hydrogen escape flux for this model is $\phi_{\text{H}_2} = 7.2 \times 10^{11} \text{ cm}^{-2} \text{ s}^{-1}$, equivalent to 82% of the diffusion-limited flux.

Fig. 4 in the main text shows the temperature and the densities of the ions and neutrals as a function of altitude. Fig. A.14 shows temperature and local volume heating and cooling rates as a function of altitude in the nominal model. At low altitudes where CO_2 is abundant, radiative heating and radiative cooling are in balance, the gas is cold, and very little energy is channeled into hydrogen escape. At high altitudes there is some radiative cooling by H_3^+ but not enough to shut off hydrogen escape. Also shown are the magnitudes of local volume heating or cooling due to thermal conduction that would be consequent to the computed temperature structure. These terms are not actually included in the model (they would of course be smaller if thermal conduction were included, because the atmosphere would adjust to smooth out the temperature profile); we plot local conductive heating and cooling here to show that thermal conduction, although not small, can be neglected at $S = 20$ for Earth without too much loss of accuracy.

Fig. A.15 shows sound speeds and flow velocities in the nominal model as a function of altitude. The flow velocity

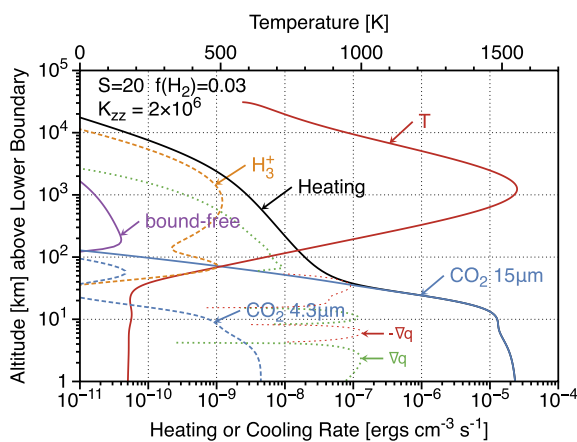


Fig. A.14. Volume heating and cooling rates in the nominal model as a function of altitude. Altitude is measured from an arbitrary lower boundary where the total density $n(r_0) = 1 \times 10^{13} \text{ cm}^{-3}$. The magnitude of the convergences and divergences of conductive heat flow – the local volume heating or cooling due to thermal conduction – are also shown.

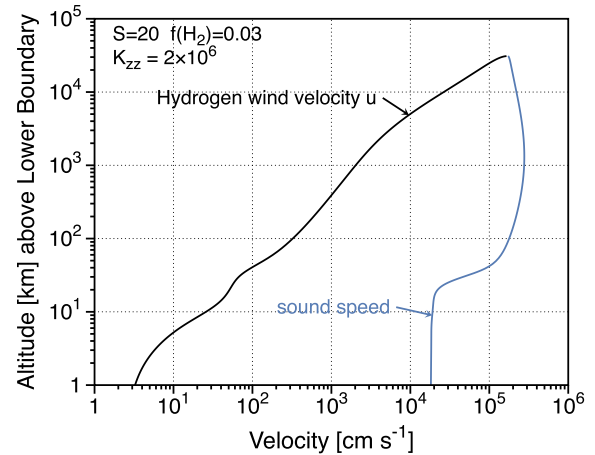


Fig. A.15. Flow velocity u and sound speed c_s as a function of altitude in the nominal model. Altitude is measured from an arbitrary lower boundary where the total density $n(r_0) = 1 \times 10^{13} \text{ cm}^{-3}$. The model stops at the critical point where $u = c_s$.

reaches the sound speed at the top of the model, which is the critical point. In the approximation we are using in this study, the gas at the critical point has exactly the minimum energy required to escape.

Fig. 5 in the main text shows the results of a parameter survey over $S - f_{\text{H}_2}$ of hydrogen escape from the $\text{CO}_2\text{-H}_2$ atmosphere for Earth, and Fig. 6 compares our results to model results previously obtained using different numerical approaches by Tian et al. (2005) and Kuramoto et al. (2013).

APPENDIX B. XENON CHEMISTRY AND TRANSPORT

B.1. Reaction rates

To compute rates of the charge transfer reactions of H^+ with neutral Xe (reactions R16a and R16b), we used the Demkov approximation (Demkov, 1964; Olson, 1972; Swartz, 1994), a variation of the Landau-Zener model applicable to singly charged ions, to calculate the cross sections σ_{16a} and σ_{16b} . The main assumption is that the charge-exchange reaction proceeds through non-local radial coupling between molecular states of the same symmetry. In contrast to the Landau-Zener model, where the coupling is assumed to be local at the internuclear distance R_x , the Demkov approximation assumes that the reaction takes place at the internuclear distance R_x through a non-local interaction well-represented by an exponential form. As is conventional in atomic physics, throughout this section we will use Hartree atomic units (a.u.), in which the electron mass, the electric charge, and the Coulomb constant are set to unity and the Planck constant is set to 2π . In a.u., the distance unit is the Bohr radius ($a_0 = 0.5291772 \text{ \AA}$). The energy unit, the Hartree, is 27.211385 eV, and is exactly twice the ionization energy of H. R_x can be determined by equating $\Delta U(R_x)$, the separation of the adiabatic electronic potentials, with

$$\Delta H(R) = H_{11}(\text{Xe} + \text{H}^+) - H_{22}(\text{Xe}^+ + \text{H}) - \Delta E, \quad (\text{B.1})$$

where $H_{11}(R)$ and $H_{22}(R)$ are incoming and outgoing adiabatic electronic interaction potentials, respectively, and $\Delta E = I_P(\text{Xe}) - I_P(\text{H}) - E_{\text{exc}}$ is the energy defect given by the difference of ionization potentials I_P of Xe and H, with $I_P(\text{Xe}) = 12.1298436$ eV and $I_P(\text{H}) = 13.6057$ eV, and E_{exc} is the energy of the final excited state of Xe^+ . The rate coefficients were calculated assuming the electronic potential model of [Sterling and Stancil \(2011\)](#). The incoming channel is

$$H_{11}(R) = -\frac{\eta_{\text{Xe}}}{2R^4} + Ae^{-(0.8+\zeta)R} \quad (\text{B.2})$$

where R is the internuclear distance, $\eta_{\text{Xe}} = 27.2903$ is the polarizability of the Xe atom in a.u. ([Lide, 2012](#)), $\zeta = 1$ is the exponent of a single orbital wave function ([Butler and Dalgarno, 1980](#)), and A is the damping amplitude, typically set to 25 ([Sterling and Stancil, 2011](#)). Similarly, the outgoing channel is given by

$$H_{22}(R) = -\frac{\eta_{\text{H}}}{2R^4} + Ae^{-(0.8+\zeta)R}, \quad (\text{B.3})$$

where the dipole polarizability of the H atom η_{H} is 9/2 in a.u. For the potential H_{11} , a quadrupole polarizability term $\pm Q_q/(2R^3)$ must be included since Xe is not initially in the ground S state ([Gentry and Giese, 1977](#); [Sterling and Stancil, 2011](#)), resulting in

$$\frac{\eta_{\text{Xe}}}{2R^4} \rightarrow \frac{\eta_{\text{Xe}}}{2R^4} - \frac{Q_q}{2R^3}, \quad (\text{B.4})$$

where the sign is selected to keep $H_{11}(R_x) - H_{22}(R_x) - \Delta E > 0$. We use $Q_q = -13.2071$ a.u., which equals -17.764 Debye \AA ([Lide, 2012](#)).

The analyzed charge exchange process is a “type I” electron capture, where the H $1s$ electron is transferred without perturbing the core electron arrangement of the ionic projectile. Consequently, $\Delta U(R_x)$ term can be estimated from the empirical fit ([Butler and Dalgarno, 1980](#))

$$\Delta U(R_x) = 27.21R_x^2 e^{-\beta R_x} \text{ eV}, \quad (\text{B.5})$$

with $\beta^2 = 2I_P(\text{Xe})$. The listed expressions are sufficient to calculate the distance R_x where the charge exchange takes place. Correct asymptotic energies for the two possible exit channels of the reaction $\text{Xe} + \text{H}^+$ are $\Delta E_{1/2} = 0.16$ eV for $\text{Xe}^+ (^2P_{1/2})$ and $\Delta E_{3/2} = 1.47$ eV for $\text{Xe}^+ (^2P_{3/2})$. For the two cases, we computed $R_x = 10.619$ a.u. and $U(R_x) = 0.1356$ eV, and $R_x = 6.935$ a.u. and $U(R_x) = 1.8746$ eV, respectively. For the averaged asymptotic shift, $\Delta E_{\text{avg}} = 1.03403$ eV, we obtained $R_x = 7.933 a_0$, confirming the result reported in [Table 1](#) in [Sterling and Stancil \(2011\)](#).

The transition probability for the charge exchange process is given by $p = e^{-w}$ ([Demkov, 1964](#); [Swartz, 1994](#)), with

$$w = \left[1 + \exp\left(\frac{2\pi^2 \Delta U(R_x)}{h\beta v}\right) \right]^{-1}, \quad (\text{B.6})$$

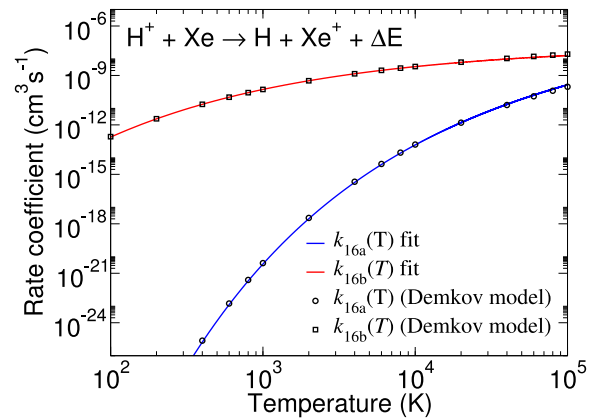


Fig. B.16. Calculated rate coefficients for the charge transfer reactions $\text{H}^+ + \text{Xe} \rightarrow \text{H} + \text{Xe}^+(^2P_{3/2})$ (R16a) and $\text{H}^+ + \text{Xe} \rightarrow \text{H} + \text{Xe}^+(^2P_{1/2})$ (R16b). Squares denote the calculated rate coefficients, the lines show the best fits to k_{16a} and k_{16b} for $50 < T < 10^5$ K. The curve fits are listed in [Table B.3](#).

where h is Planck’s constant and v is the relative velocity of the interacting particles. The charge exchange cross section is given by ([Olson, 1972](#); [Swartz, 1994](#))

$$\sigma_x(E) = \pi R_x^2 \int_1^\infty \frac{dx}{x^3} \frac{4e^{-\delta x}}{(1 + e^{-\delta x})^2}, \quad (\text{B.7})$$

where

$$\delta = \frac{\pi^2 \Delta U(R_x)}{h\beta v}. \quad (\text{B.8})$$

Finally, the charge exchange rate coefficient at temperature T can be expressed as $k(T) = \langle \sigma_x v \rangle$, where $\langle \dots \rangle$ implies averaging over a Maxwell-Boltzmann distribution of initial collision velocities. Numerically evaluated rates are shown in [Fig. B.16](#) for temperatures between $100 - 10^6$ K. We constructed fits to $k(T) = AT^b \exp(-c/T^d)$, with two sets of coefficients depending on the exit channel: $A = 3.83017 \times 10^{-8} \text{ cm}^3 \text{ s}^{-1}$, $b = 0.038557$, $c = 55.7906 \text{ K}^d$, $d = 0.326$ (for $\Delta E_{1/2}$) and $A = 2.37109 \times 10^{-9} \text{ cm}^3 \text{ s}^{-1}$, $b = 0.342427$, $c = 294.089 \text{ K}^d$, $d = 0.3332$ (for $\Delta E_{3/2}$). The uncertainty of rates calculated using the Demkov approximation has been shown to be less than a factor of three for rates larger than about $10^{-9} \text{ cm}^3 \text{ s}^{-1}$ ([Butler and Dalgarno, 1980](#); [Kingdon and Ferland, 1996](#)), which is good enough for our purposes.

Xenon reaction rates used here are listed in [Table B.3](#).

B.2. Collision frequencies

The ion-ion collision frequency for momentum transfer is ([Schunk and Nagy, 1980](#))

$$v_{ij} \approx 1.27 \frac{z_i^2 z_j^2 A_{ij}^{0.5}}{A_i} \frac{n_j}{T_{ij}^{1.5}} \quad (\text{B.9})$$

where z_i and z_j are the charges of the ions (integers), and A_i and A_{ij} are the mass and the reduced mass in amu,

Table B.3
Summary of Xe Chemistry.

Label	Reactants	Products	Rate [$\text{cm}^3 \text{s}^{-1}$]
JXe	$\text{Xe} + h\nu$	$\rightarrow \text{Xe}^+ + e^-$	J_{Xe}
R15	$\text{CO}_2^+ + \text{Xe}$	$\rightarrow \text{CO}_2 + \text{Xe}^+$	$k_{15} = 6 \times 10^{-10}$
R16a	$\text{H}^+ + \text{Xe}$	$\rightarrow \text{H} + \text{Xe}^+ (^2\text{P}_{3/2})$	$k_{16a} = 2.37 \times 10^{-9} T^{0.342} e^{-294/T^{0.333}}$
R16b	$\text{H}^+ + \text{Xe}$	$\rightarrow \text{H} + \text{Xe}^+ (^2\text{P}_{1/2})$	$k_{16b} = 3.83 \times 10^{-8} T^{0.386} e^{-55.8/T^{0.326}}$
R17	$\text{Xe}^+ + \text{O}_2$	$\rightarrow \text{Xe} + \text{O}_2^+$	$k_{17} = 1.2 \times 10^{-10}$
R17r	$\text{O}_2^+ + \text{Xe}$	$\rightarrow \text{O}_2 + \text{Xe}^+$	$k_{17r} = 3 \times 10^{-10} e^{-500/T}$
R18	$\text{Xe}^+ + e^-$	$\rightarrow \text{H} + h\nu$	$k_{18} = k_5$

Table B.4
Binary diffusion coefficients for Xe.

Symbol	i, j	$b(i, j) \text{ cm}^{-1} \text{ s}^{-1}$	Reference
b_{23}	H_2, CO_2	$4.0 \times 10^{19} (T/1000)^{0.71}$	Marrero and Mason (1972)
b_{2j}	H_2, Xe	$1.8 \times 10^{19} (T/1000)^{0.71}$	Marrero and Mason (1972)
b_{1j}	H, Xe	$2.6 \times 10^{19} (T/1000)^{0.71}$	scaled from b_{2j}
b_{3j}	CO_2, Xe	$4.0 \times 10^{18} (T/1000)^{0.75}$	scaled from $b(\text{CO}_2, \text{SF}_6)$
b_{1j}^+	H, Xe^+	$3.9 \times 10^{19} (T/1000)$	Eq. (B.12), $\eta_n(\text{H}) = 0.6668 \text{ \AA}^3$
b_{2j}^+	H_2, Xe^+	$1.6 \times 10^{19} (T/1000)$	Eq. (B.12), $\eta_n(\text{H}_2) = 0.9 \text{ \AA}^3$
b_{3j}^+	CO_2, Xe^+	$3.3 \times 10^{18} (T/1000)$	Eq. (B.12), $\eta_n(\text{CO}_2) = 2.9 \text{ \AA}^3$
b_{1j}^{++}	H^+, Xe^+	$2.1 \times 10^{15} (T/1000)^{2.5}$	Eq. (B.10).
b_{4j}^{++}	$\text{CO}_2^+, \text{Xe}^+$	$6.4 \times 10^{13} (T/1000)^{2.5}$	Eq. (B.10).
b_{5j}^{++}	$\text{HCO}^+, \text{Xe}^+$	$8.9 \times 10^{13} (T/1000)^{2.5}$	Eq. (B.10).
Not used	H^+, Xe	$1.6 \times 10^{19} (T/1000)$	Eq. (B.12), $\eta_n(\text{Xe}) = 4.05 \text{ \AA}^3$

respectively. The mapping between momentum transfer collision frequencies ν_{ij} and binary diffusion coefficients is given by Eq. (A.29). For Xe^+ and H^+ ,

$$b_{1j}^{++} \approx \frac{k_B T^{2.5}}{1.27 m_1} = 2.1 \times 10^{15} (T/1000)^{2.5} \text{ cm}^{-1} \text{ s}^{-1}. \quad (\text{B.10})$$

The b_{ij}^{++} are much smaller (Table B.4) for the heavy molecular ions HCO^+ and CO_2^+ because the reduced masses are much larger.

Less important are interactions between ions and neutrals, but we include these for completeness. The ion-neutral collision frequency for momentum transfer is (Schunk and Nagy, 1980)

$$\nu_{in} = 2.21 \pi \frac{n_n m_n}{m_i + m_n} \left(\frac{\eta_n e^2}{\mu_{in}} \right)^{0.5}. \quad (\text{B.11})$$

Written as a binary diffusion coefficient,

$$b_{in}^+ = \frac{k_B T}{2.21 \pi e \sqrt{\mu_{in} \eta_n}} \quad (\text{B.12})$$

where μ_{in} is the reduced mass, e the electric charge, and η_n the polarizability of the neutral. Unless the gas is cold, the ion-neutral cross sections are not much larger than the corresponding neutral-neutral cross sections.

Beginning from Eq. (A.30), with appropriate substitutions and with the ν_j^2 terms ignored, an equation describing the several forces acting on Xe^+ is

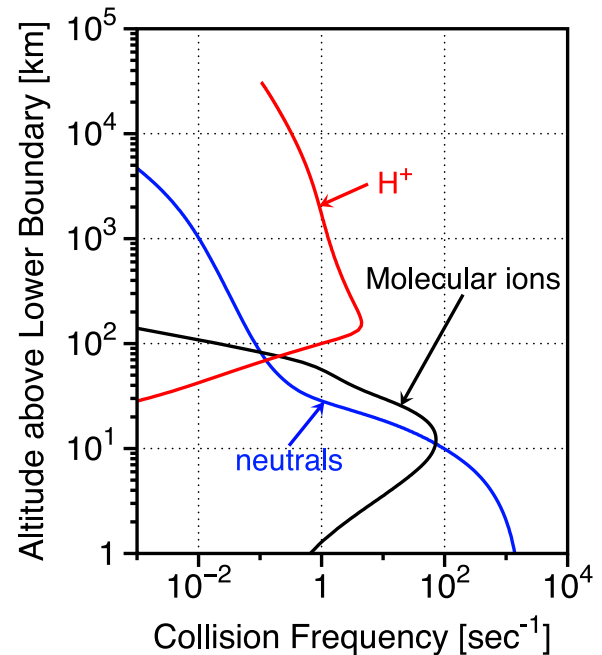


Fig. B.17. Momentum transfer collision frequencies ν_{ij} of Xe^+ with neutrals, molecular ions, and H^+ in the nominal model ($f_{\text{H}_2} = 0.03, S = 20$). Altitude is measured from an arbitrary lower boundary where the total density $n(r_0) = 1 \times 10^{13} \text{ cm}^{-3}$. Xe^+ transport takes place in three regimes. The homopause is at $\sim 4 \text{ km}$. Below the homopause Xe^+ transport is collisionally dominated by neutral molecules. Between 10 km and 80 km (the baropause), the Xe^+ ions are collisionally dominated by molecular ions stemming from CO_2 . Above 80 km, Xe^+ is most responsive to the outbound flow of H^+ .

$$\begin{aligned}
& \left(1 + \sum_i \frac{K_{zz} n_i}{b_{ij}^+} + \sum_i \frac{K'_{zz} x_i}{b_{ij}^{++}} \right) \left(\frac{1}{x_j} \frac{\partial x_j}{\partial r} + \frac{1}{T} \frac{\partial T}{\partial r} \right) \\
& = -(v_j - u) \left(\frac{n_1}{b_{1j}^+} + \frac{n_2}{b_{2j}^+} \right) \\
& - \frac{GM_{\oplus}}{r^2 k_B T} \left(m_j - \frac{\mu^+}{2} + \sum_i \frac{K_{zz} n_i \mu}{b_{ij}^+} + \sum_i \frac{K'_{zz} x_i m_i^+}{b_{ij}^{++}} \right) \\
& - v_j \sum_i \frac{x_i}{b_{ij}^{++}} - v_j \frac{n_3}{b_{3j}^+} \quad (\text{B.13})
\end{aligned}$$

Save near the lower boundary, the upward force on Xe^+ is dominated by the ion-ion interactions. Eq. (B.13) is recast as an equation for $\partial v_j / \partial r$ that is readily integrated numerically beginning at the lower boundary

$$\begin{aligned}
\frac{1}{v_j} \frac{\partial v_j}{\partial r} &= \frac{1}{T} \frac{\partial T}{\partial r} - \frac{2}{r} + \frac{GM_{\oplus}}{r^2 k_B T} \frac{m_j - \mu^+ + A_a \mu + A_b m_4^+ + A_c m_5^+}{A_d} \\
& + \frac{v_j - u}{A_d} \left(\frac{n_1}{b_{1j}^+} + \frac{n_2}{b_{2j}^+} \right) + \frac{v_j}{A_d} \frac{n_3}{b_{3j}^+} + \frac{v_j - u}{A_d} \frac{x_1}{b_{1j}^{++}}. \quad (\text{B.14})
\end{aligned}$$

where

$$\begin{aligned}
A_a &= \sum_i \frac{K_{zz} n_i}{b_{ij}^+} & A_b &= \frac{K'_{zz} x_4}{b_{4j}^+} & A_c &= \frac{K'_{zz} x_5}{b_{5j}^+} \\
A_d &= A_a + A_b + A_c + 1
\end{aligned}$$

Eq. (B.14) is solved by the shooting method. The velocity $v_j(r)$ is integrated upward from the lower boundary for all the Xe isotopes. The lower boundary velocity $v_j(r_0)$ is bounded by 0 and by the hydrogen velocity $u(r_0)$ (i.e., Xe cannot escape more easily than hydrogen). The velocity $v_j(r_0)$ at the lower boundary is iterated until either

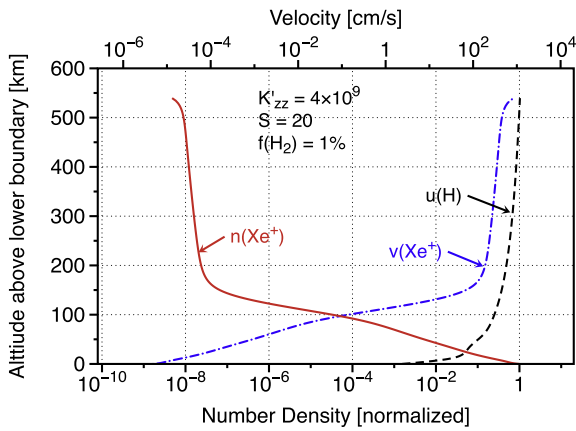


Fig. B.18. An example of Xe^+ ions dragged to space by ionized hydrogen. Ion number density (red, labeled $n(\text{Xe}^+)$) is normalized to unity at the lower boundary. Xe^+ velocities (blue, labeled $v(\text{Xe}^+)$) are compared to the hydrogen velocity (black, labeled $u(\text{H})$). Velocities and densities are mirror images because the flux $x_j v_j r^2$ is conserved by construction. Altitude is measured from an arbitrary lower boundary where the total density $n(r_0) = 1 \times 10^{13} \text{ cm}^{-3}$. (For interpretation of the references to color in this figure legend, the reader is referred to the web version of this article.)

$v_j(r) \rightarrow u(r)$, in which case Xe^+ escapes, or $v_j(r) \rightarrow 0$, in which case Xe^+ is hydrostatic and does not escape.

Fig. B.18 documents the vertical structure of Xe^+ ions in the nominal model ($S = 20, f_{\text{H}_2} = 0.03, K_{zz} = 2 \times 10^6$, and $K'_{zz} = 4 \times 10^9 \text{ cm}^2 \text{ s}^{-1}$) and three variants ($S = 40, f_{\text{H}_2} = 0.01$, and $K'_{zz} = 4 \times 10^8 \text{ cm}^2 \text{ s}^{-1}$). In all four models Xe^+ is dragged to space by ionized hydrogen. The Xe^+ number densities x_j are normalized to $x_j(r_0) = 1$ at the lower boundary. The figure illustrates the sensitivity of Xe^+ to vertical transport amongst the molecular ions (parameterized by K'_{zz}), to the solar XUV flux S , and to the hydrogen mixing ratio at the lower boundary f_{H_2} .

APPENDIX C. TABLE OF SYMBOLS

Symbol	Definition
A_a, A_b, A_c, A_d	mixing parameters of neutral atmosphere and molecular ionosphere
A_s, A_{st}	mass and reduced mass (amu)
A_{v_2}	spontaneous emission rate for 15 μm (v_2) CO_2 band [s^{-1}]
A_{v_3}	spontaneous emission rate for 4.3 μm (v_3) CO_2 band [s^{-1}]
a	the power of XUV decay $S(t) \propto t^{-1}$
a_0	Bohr radius, $a_0 = 0.529177 \text{ \AA}$. $a_0 \equiv 1$ in atomic units.
a_1, a_2, a_3	curve fit parameters for $\Gamma_{\text{H}_3^+}$
A_{\oplus}	area of Earth (cm^2)
B, B_{\oplus}	geomagnetic field; $B_{\oplus} = 0.31$ Gauss
b_{ij}	binary diffusivity between species i and j [$\text{cm}^{-1} \text{ s}^{-1}$]
b_{ij}^+	binary diffusivity between an ion i and a neutral j [$\text{cm}^{-1} \text{ s}^{-1}$]
b_{ij}^{++}	binary diffusivity between two ions i and j [$\text{cm}^{-1} \text{ s}^{-1}$]
$\bar{b} = b_{23}$	the binary diffusivity pertinent to the homopause [$\text{cm}^{-1} \text{ s}^{-1}$]
c	speed of light [cm s^{-1}]
$c_s = \sqrt{\gamma k_B T / \mu}$	speed of sound [cm s^{-1}]
$c'^2 = \frac{k_B T}{\mu'} \left(1 + \frac{K_{zz} n}{b} \right)$	a kind of sound speed in hydrogen, squared
$E(\tau_x)$	dimensionless function, Kumer & James $E(x)$
e	electron charge [4.8×10^{-10} statcoulombs]
e_s	specific energy of the gas [ergs g^{-1}]
F_{fuv}	total FUV irradiation ($91.2 < \lambda < 200 \text{ nm}$) [$\text{ergs cm}^{-2} \text{ s}^{-1}$]
F_{xuv}	total XUV irradiation ($\lambda < 91.2 \text{ nm}$) [$\text{ergs cm}^{-2} \text{ s}^{-1}$]
F_{λ}	incident photon flux [$\text{cm}^{-2} \text{ s}^{-1}$] in wavelength bin centered on λ
$f_i = n_i / N$	mixing ratio of species i
f_{H_2}	total mixing ratio of hydrogen at the lower boundary
G	universal gravitational constant [$\text{cm}^3 \text{ g}^{-1} \text{ s}^{-2}$]
H	scale height of atmosphere [cm]
$H_{11} (H_{22})$	incoming (outgoing) adiabatic electronic interaction potential [eV]
h	Planck's constant [ergs s]

I_P	ionization potential [eV]	Γ_{15}	CO ₂ cooling at 15 μm [ergs $\text{cm}^{-3} \text{s}^{-1}$]
J_{in}	photolysis rate of species i , pathway n [s^{-1}]	$\Gamma_{4.3}$	CO ₂ cooling at 4.3 μm [ergs $\text{cm}^{-3} \text{s}^{-1}$]
J'_3	weighted photolysis rate of CO ₂ for splitting H ₂ [s^{-1}]	γ_i	ratio of specific heats of species i
J_{Xe}	photo-ionization rate of Xenon i [s^{-1}]	η	net heating efficiency for energy-limited escape
K_{zz}	Eddy diffusivity of lower atmosphere near homopause [$\text{cm}^2 \text{s}^{-1}$]	η_h	radiative heating efficiency
K'_{zz}	Eddy diffusivity of ions in the molecular ionosphere [$\text{cm}^2 \text{s}^{-1}$]	η_n	dipole polarizability [cm^3]
k_B	Boltzmann constant [ergs K^{-1}]	$\Theta(\Lambda, \tau_x)$	dimensionless function, Kumer & James $F(\lambda, x)$
k_c	thermal conductivity [ergs $\text{cm}^{-1} \text{s}^{-1} \text{K}^{-1}$]	Λ	dimensionless parameter, Kumer & James λ
k_i^*	collisional de-excitation rate of CO ₂ by species i [$\text{cm}^3 \text{s}^{-1}$]	λ	wavelength of light
k_n	rate of reaction n [$\text{cm}^3 \text{s}^{-1}$]	$\mu = \sum_i n_i m_i / n$	mean molecular mass [g]
M_\oplus	mass [g] of Earth	μ_{ij}	reduced mass between two species i and j [g]
$M_{\text{H}_2\text{O}}$	equivalent mass of water corresponding to lost H ₂ [g]	$\mu' = \rho' / (n_1 + n_2)$	hydrogen mean molecular mass [g]
\dot{M}_{sw}	solar wind flux [g $\text{cm}^{-2} \text{s}^{-1}$]	$\mu^+ = \sum_i x_i m_i / n_e$	mean molecular mass of ions [g]
m_i	mass of species i [g]	ν_{ij}	collision frequency for momentum transfer [s^{-1}]
m_i^+	mass of ion i [g]	ν_{in}	ion-neutral collision frequency for momentum transfer [s^{-1}]
$m_{\text{H}_2} = m_2$	mass of molecule H ₂ [g]	ν_{st}	ion-ion collision frequency for momentum transfer [s^{-1}]
N_a	column density of atmosphere [number cm^{-2}]	ξ_j	depletion (total escape) of Xe isotope j
N_{H_2}	column density of H ₂ [number cm^{-2}]	ξ_{ij}	fractionation (per amu) between ¹³⁰ Xe and ¹³¹ Xe.
N_j	column density of ^{j} Xe [number cm^{-2}]	$\rho' = n_1 m_1 + n_2 m_2$	total hydrogen density [g cm^{-3}]
$n = \sum_i n_i$	total number density [cm^{-3}]	σ_x	charge exchange cross-section [a_0^2 in a.u.]
$n_e = \sum_i x_i$	electron density [cm^{-3}]	$\sigma_{i\lambda}$	absorption cross-section species i at wavelength λ [cm^2]
n_i	number density of species i [cm^{-3}]	σ_{v_2}	effective cross section for 15 μm (ν_2) CO ₂ band [cm^2]
Q	thermal conduction flux [ergs $\text{cm}^{-2} \text{s}^{-1}$]	σ_{v_3}	effective cross section for 4.3 μm (ν_3) CO ₂ band [cm^2]
Q_q	quadrupole polarizability [Debye \AA]	$\tau_{i\lambda}$	optical depth of species i at wavelength λ
R_\oplus	radius [cm] of Earth	$\tau_\lambda = \sum_i \tau_{i\lambda}$	total optical depth at wavelength λ
R, R_x	internuclear distance, [a_0] in atomic units	τ_x	line center optical depth, Kumer & James x
r	radial distance [cm]	ϕ_i	flux of species or isotope i [$\text{cm}^{-2} \text{s}^{-1}$]
r_0	radius to lower boundary of the model [cm]	$\phi_{\text{H}_2} = 0.5\phi_1 + \phi_2$	total hydrogen escape flux [$\text{cm}^{-2} \text{s}^{-1}$]
$S \equiv F_{\text{xuv}} / F_{\text{xuv}\oplus}$	XUV/FUV irradiation relative to modern Earth	ϕ_{DL}	diffusion limited flux ϕ_{H_2} [$\text{cm}^{-2} \text{s}^{-1}$]
T	temperature [K]	ϕ_{EL}	energy limited flux ϕ_{H_2} [$\text{cm}^{-2} \text{s}^{-1}$]
t	time [Gyr]		
t_A, t_B	starting and ending times [Gyr] of a period of Xe fractionation		
$u = v_1 = v_2$	uniform outward mean velocity of hydrogen [cm s^{-1}]		
v_i	outward mean velocity of species i [cm s^{-1}]		
v_{sw}	solar wind velocity [cm s^{-1}]		
x_i	number density of ion i [cm^{-3}]		
$z = r - r_0$	altitude [cm]		
z_s, z_i	ionic charge		
α	the α parameter in accretion disk theory		
α_j	escape factor for Xe isotope j		
$\alpha_{ij} \equiv \alpha_{130} - \alpha_{131}$	fractionation factor between Xe isotopes separated by 1 amu		
β, U, w, δ	charge exchange parameters		
Γ_h	total volume radiative heating [ergs $\text{cm}^{-3} \text{s}^{-1}$]		
Γ_c	total volume radiative cooling [ergs $\text{cm}^{-3} \text{s}^{-1}$]		
$\Gamma_{\text{H}_3^+}$	broadband H ₃ ⁺ cooling [ergs $\text{cm}^{-3} \text{s}^{-1}$]		
Γ_{bf}	bound-free cooling by H ⁺ [ergs $\text{cm}^{-3} \text{s}^{-1}$]		
Γ_{ff}	free-free cooling by H ⁺ [ergs $\text{cm}^{-3} \text{s}^{-1}$]		

REFERENCES

- Alexander C. M. O. D., Bowden R., Fogel M. L., Howard K. T., Herd C. D. K. and Nittler L. R. (2012) The provenances of asteroids, and their contributions to the volatile inventories of the terrestrial planets. *Science* **337**, 721–723.
- Anicich V. G. (1993) A survey of bimolecular ion-molecule reactions for use in modeling the chemistry of planetary atmospheres, cometary comae, and interstellar clouds. *Astrophys. J. Supp.* **84**, 215–315.
- Anicich V. G. and Huntress W. T. (1986) A survey of bimolecular ion-molecule reactions for use in modeling the chemistry of planetary atmospheres, cometary comae, and interstellar clouds. *Astrophys. J. Supp.* **62**, 553–672.
- Allen D. C., Scragg T. and Simpson C. J. S. M. (1980) Low temperature fluorescence studies of the deactivation of the bend-stretch manifold of CO₂. *Chem. Phys.* **51**, 279–298.

- Arney G., Domagal-Goldman S. D., Meadows V. S., Wolf E. T., Schwieterman E., Charnay B., Claire M., Hébrard E. and Trainer M. G. (2016) The pale orange dot: the spectrum and habitability of hazy archaic earth. *Astrobiology* **16**, 873–899.
- Aston F. W. (1924) The rarity of the inert gases on Earth. *Nature* **114**, 786.
- Atreya S. K., Mahaffy P. R., Niemann H. B., Wong M. H. and Owen T. C. (2003) Composition and origin of the atmosphere of Jupiter? An update, and implications for the extrasolar giant planets. *Planet. Space Sci.* **51**, 105–112.
- Aulbach S., Woodland A. B., Vasilyev P., Galvez M. E. and Viljoen K. S. (2017) Effects of low-pressure igneous processes and subduction on $\text{Fe}_3^+/\Sigma\text{Fe}$ and redox state of mantle eclogites from Lace (Kaaresvika craton). *Earth Planet. Sci. Lett.* **474**, 283–295.
- Avicé G., Marty B., Hofmann A., Zahnle K. J., Philippot P. and Zakharov D. (2018) Evolution of atmospheric xenon and other noble gases inferred from the study of Archaean to Paleoproterozoic rocks. *Geochim. Cosmochim. Acta* **232**, 82–100.
- Bekaert D. V., Broadley M. W., Delarue F., Avicé G., Robert F. and Marty B. (2018) Archaean kerogen as a new tracer of atmospheric evolution: implications for dating the widespread nature of early life. *Sci. Adv.* **4**, eaar2091.
- Biggin A. J., Piispa E. J., Pesonen L. J., Holme R., Paterson G. A., Veikkolainen T. and Tauxe L. (2015) Palaeomagnetic field intensity variations suggest Mesoproterozoic inner-core nucleation. *Nature* **526**, 245–248.
- Bolmont E., Selsis F., Owen J. E., Ribas I., Raymond S. N., Lecante J. and Gillon M. (2017) Water loss from terrestrial planets orbiting ultracool dwarfs: implications for the planets of TRAPPIST-1. *Mon. Not. Roy. Astron. Soc.* **464**, 3728–3741.
- Bougher S. W., Hunten D. M. and Roble R. G. (1994) CO_2 cooling in terrestrial planet thermospheres. *J. Geophys. Res.* **99**, 14609–14622.
- Brown H. (1949) Rare gases and the formation of the Earth's atmosphere. In *The Atmosphere of the Earth and Planets* (ed. G. Kuiper). Univ. Chicago Press, Chicago, pp. 258–266.
- Butler S. E. and Dalgarno A. (1980) Charge transfer of multiply charged ions with hydrogen and helium Landau-Zener calculations. *Astrophys. J.* **241**, 838–843.
- Cassata W. S. (2017) Meteorite constraints on Martian atmospheric loss and paleoclimate Earth Planet. Sci. Lett. **479**, 322–329.
- Catling D. C., Zahnle K. J. and McKay C. P. (2001) Biogenic methane, hydrogen escape, and the irreversible oxidation of early Earth. *Science* **293**, 839–843.
- Catling D. C. and Kasting J. F. (2017) *Atmospheric Evolution on Inhabited and Lifeless Worlds*. Cambridge University Press, p. 592.
- Claire M. W., Sheets J., Cohen M., Ribas I., Meadows V. S. and Catling D. C. (2012) The evolution of solar flux from 0.1 nm to 160 μm : quantitative estimates for planetary studies. *Astrophys. J.* **757**, 95.
- Cottrell E. and Kelley K. A. (2011) The oxidation state of Fe in MORB glasses and the oxygen fugacity of the upper mantle. *Earth Planet. Sci. Lett.* **305**, 270–282.
- Dauphas N. (2003) The dual origin of the terrestrial atmosphere. *Icarus* **165**, 326–339.
- Dauphas N. and Morbidelli A. (2014). Geochemical and planetary dynamical views on the origin of Earth's atmosphere and oceans. *Treatise in Geochemistry 2nd Edition* <https://doi.org/10.1016/B978-0-08-095975-7.01301-2>.
- Demkov Yu. N. (1964) Charge transfer at small resonance defects. *Sov. Phys. JETP* **18**, 138.
- Domagal-Goldman S. D., Kasting J. F., Johnston D. T. and Farquhar J. (2008) Organic haze, glaciations and multiple sulfur isotopes in the Mid-Archaean Era. *Earth Planet. Sci. Lett.* **269**, 29–40.
- Fegley B. (2003) *Venus Treatise on Geochemistry*, vol. 1. Elsevier, pp. 487–507.
- Frick U., Mack R. and Chang S. (1979) Noble gas fractionation during synthesis of carbonaceous matter. *Proc. Lunar Planet. Sci. Conf. X*, 405–407.
- Frost D. J. and McCammon C. A. (2008) The redox state of Earth's mantle. *Annu. Rev. Earth Planet. Sci.* **36**, 389–420.
- Gentry W. R. and Giese C. F. (1977) Long-range interactions of ions with atoms having partially filled p subshells. *J. Chem. Phys.* **5**, 2355–2361.
- Gordiets B. F., Kulikov Yu. N., Markov M. N. and Marov M. Ya. (1982) Numerical modeling of the thermosphere heat budget. *J. Geophys. Res.* **87**, 4504–4514.
- Gross S. H. (1972) On the exospheric temperature of hydrogen-dominated planetary atmospheres. *J. Atmos. Sci.* **29**, 214–219.
- Hashimoto G. L., Abe Y. and Seiji Sugita S. (2007) The chemical composition of the early terrestrial atmosphere: formation of a reducing atmosphere from CI-like material. *J. Geophys. Res.* **112**, E05010. <https://doi.org/10.1029/2006JE002844>.
- Hayes J. M. (1994) Global methanotrophy at the Archaean-Proterozoic transition. In *Early Life on Earth, Nobel Symposium 84* (ed. S. Bengtson), pp. 220–236.
- Hébrard E. and Marty B. (2014) Coupled noble gas-hydrocarbon evolution of the early Earth atmosphere upon solar UV irradiation. *Earth Planet. Sci. Lett.* **385**, 40–48.
- Hinrichs K.-U. (2002) Microbial fixation of methane carbon at 2.7 Ga: was an anaerobic mechanism possible? *Geochem. Geophys. Geosyst.* **3**. <https://doi.org/10.1029/2001GC000286>.
- Holland G., Cassidy M. and Ballentine C. J. (2009) Meteorite Kr in Earth's mantle suggests a late accretionary source for the atmosphere. *Science* **326**, 1522–1525.
- Holland G., Sherwood-Lollar B., Li L., Lacrampe-Couloume G., Slater G. F. and Ballentine C. J. (2013) Deep fracture fluids isolated in the crust since the Precambrian era. *Nature* **497**, 357–360.
- Huebner W. F., Keady J. J. and Lyon S. P. (1992) Solar photo rates for planetary atmospheres and atmospheric pollutants. *Astrophys. Space Sci.* **195**, 1–294.
- Hunten D. M. (1973) The escape of light gases from planetary atmospheres. *J. Atmos. Sci.* **30**, 1481–1494.
- Hunten D. M., Pepin R. O. and Walker J. C. G. (1987) Mass fractionation in hydrodynamic escape. *Icarus* **69**, 532–549.
- Huntress W. T. (1977) Laboratory studies of bimolecular reactions of positive ions in interstellar clouds, in comets, and in planetary atmospheres of reducing composition. *Astrophys. J. Supp.* **33**, 495–514.
- Ishii M. (2005) Relationship between thermospheric vertical wind and the location of ionospheric current in the polar region. *Adv. Polar Upper Atmos. Res.* **19**, 63–70.
- Izon G., Zerkle A. L., Williford K. H., Farquhar J., Poulton S. W. and Claire M. W. (2017) Biological regulation of atmospheric chemistry en route to planetary oxygenation. *PNAS* **114**, E2571–E2579.
- James T. C. and Kumer J. B. (1973) Fluorescence of CO_2 near 4.3 microns. *J. Geophys. Res.* **78**, 6151.
- Kasting J. F. (1990) Bolide impacts and the oxidation state of carbon in the Earth's early atmosphere. *Orig. Life Evol. Biosph.* **20**, 199–231.
- Kasting J. F. and Pollack J. B. (1983) Loss of water from Venus. I. Hydrodynamic escape of hydrogen. *Icarus* **53**, 479–508.
- King A. R., Pringle J. E. and Livio M. (2007) Accretion disc viscosity: how big is alpha? *Mon. Not. Roy. Astron. Soc.* **376**, 1740–1746.

- Kingdon J. B. and Ferland G. J. (1996) Rate coefficients for charge transfer between hydrogen and the first 30 elements. *Astrophys. J. Supp.* **106**, 205.
- Korenaga J., Planovsky N. and Evans D. A. D. (2017) Global water cycle and coevolution of Earth's interior and surface environment. *Phil. Trans. Roy. Soc. A* **375**, 20150393.
- Koskinen T. T., Lavvas P., Harris M. J. and Yelle R. V. (2014) Thermal escape from extrasolar giant planets. *Phil. Trans. Roy. Soc. A* **372**, 20130089, 12 pp.
- Krems R. V., Jamieson M. J. and Dalgarno A. (2006) The ^1D - ^3P transitions in atomic oxygen induced by impact with atomic hydrogen. *Astrophys. J.* **647**, 1531–1534.
- Kulikov Y. N., Lammer H., Lichtenegger H. I. M., Penz T., Breuer D., Spohn T., Lundin R. and Biernat H. K. (2007) A comparative study of the influence of the active young Sun on the early atmospheres of Earth, Venus, and Mars. *Space Sci. Rev.* **129**, 207–243.
- Kumer J. B. and James T. C. (1974) $\text{CO}_2(001)$ and N_2 vibrational temperatures in the $50 < z < 130$ km altitude range. *J. Geophys. Res.* **79**, 638.
- Kuramoto K., Umemoto T. and Ishiwatari M. (2013) Effective hydrodynamic hydrogen escape from an early Earth atmosphere inferred from high-accuracy numerical simulation. *Earth Planet. Sci. Lett.* **375**, 312–318.
- Lammer H., Erkaev N. V., Odert P., Kislyakova K. G., Leitzinger M. and Khodachenko M. L. (2013) Probing the blow-off criteria of hydrogen-rich 'super-Earths'. *Mon. Not. Roy. Astron. Soc.* **430**, 1247–1256.
- Larsen M. F. and Meriwether J. W. (2012) Vertical winds in the thermosphere. *J. Geophys. Res.* **117**, A09319. <https://doi.org/10.1029/2012JA017843>.
- Lide D. R. (2012) *CRC Handbook of Chemistry and Physics: A Ready-reference Book of Chemical and Physical Data*. CRC Press, Boca Raton.
- Lowe D. and Byerly G. (2018) The terrestrial record of Late Heavy Bombardment. *New Astron. Rev.* **81**, 39–61.
- Marrero T. R. and Mason E. A. (1972) Gaseous diffusion coefficients. *J. Phys. Chem. Ref. Data* **1**, 2–118.
- Marrocchi Y. and Marty B. (2013) Experimental determination of the xenon isotopic fractionation during adsorption. *Geophys. Res. Lett.* **40**, 4165–4170.
- Marrocchi Y., Marty B., Reinhardt P. and Robert F. (2011) Adsorption of xenon ions onto defects in organic surfaces: implications for the origin and the nature of organics in primitive meteorites. *Geochim. Cosmochim. Acta* **75**, 6255–6266.
- Marty B. et al. (2017) Xenon isotopes in 67P/Churyumov-Gerasimenko show that comets contributed to Earth's atmosphere. *Science* **356**, 1069–1072.
- McElroy D., Walsh C., Markwick A. J., Cordiner M. A., Smith K. and Millar T. J. (2012) The UMIST database for astrochemistry 2012. *Astron. Astrophys.* **550**, id.A36, 13 pp.
- Mendillo M., Withers P. and Dalba P. A. (2018) Atomic oxygen ions as ionospheric biomarkers on exoplanets. *Nature Astron.* <https://doi.org/10.1038/s41550-017-0375-y>.
- Meshik A. P., Hohenberg C. M., Pravdivtseva O. V. and Burnett D. (2014) Heavy noble gases in solar wind delivered by Genesis mission. *Geochim. Cosmochim. Acta* **127**, 326–347.
- Murray-Clay R. A., Chiang E. I. and Murray N. (2009) Atmospheric escape from hot Jupiters. *Astrophys. J.* **693**, 23–42.
- Neale L., Miller S. and Tennyson J. (1996). *Astrophys. J.* **464**, 516–520.
- Nicklas R. W., Puchtel I. S. and Ash R. D. (2018) Redox state of the Archean mantle: evidence from V partitioning in 3.5–2.4 Ga komatiites. *Geochim. Cosmochim. Acta* **222**, 447–466.
- Olson R. E. (1972) Charge transfer at large internuclear distances: application to asymmetric alkali-ion-alkali-atom systems. *Phys. Rev. A* **6**, 1822–1830.
- Ozaki K., Tajika E., Hong P. K., Nakagawa Y. and Reinhard C. T. (2018) Effects of primitive photosynthesis on Earth's early climate system. *Nat. Geosci.* **11**, 55–59.
- Ozima M., Seki K., Terada N., Miura Y. N., Podosek F. A. and Shinagawa H. (2005) Terrestrial nitrogen and noble gases in lunar soils. *Nature* **436**, 655–659.
- Ozima M. and Podosek F. A. (1983) *Noble Gas Geochemistry*. Cambridge University Press, 367 pp.
- Pepin R. O. (1991) On the origin and early evolution of terrestrial planet atmospheres and meteoritic volatiles. *Icarus* **92**, 2–79.
- Pepin R. O. (2000) On the isotopic composition of primordial xenon in terrestrial planet atmospheres. *Space Sci. Rev.* **92**, 371–395.
- Pepin R. O. (2006) Atmospheres on the terrestrial planets: clues to origin and evolution. *Earth Planet. Sci. Lett.* **252**, 1–14.
- Pepin R. O. (2013) Comment on "Chondritic-like xenon trapped in Archean rocks: A possible signature of the ancient atmosphere" by Pujol, M., Marty, Burgess, R., Earth and Planetary Science Letters 308 (2011) 298–306. *Earth Planet. Sci. Lett.* **271–272**, 294–295.
- Pope E. C., Bird D. K. and Rosing M. T. (2012) Isotope composition and volume of Earth's early oceans. *Proc. Nat. Acad. Sci.* **109**, 4371–4376.
- Pujol M., Marty B., Burnard P. and Phillipot P. (2009) Xenon in Archean barite: weak decay of ^{130}Ba , mass-dependent isotopic fractionation and implication for barite formation. *Geochim. Cosmochim. Acta* **73**, 6834–6846.
- Pujol M., Marty B. and Burgess R. (2011) Chondritic-like xenon trapped in Archean rocks: a possible signature of the ancient atmosphere. *Earth Planet. Sci. Lett.* **308**, 298–306.
- Pujol M., Marty B. and Burgess R. (2013) Reply to comment on "Chondritic-like xenon trapped in Archean rocks: A possible signature of the ancient atmosphere" by Pujol, M., Marty, B., Burgess, R., Earth and Planetary Science Letters 308 (2011) 298–306 by Pepin, R.O.". *Earth Planet. Sci. Lett.*, 296–298.
- Ribas I., Guinan E. F., Güdel M. and Audard M. (2005) Evolution of the solar activity over time and effects on planetary atmospheres. I. High-energy irradiances (1–1700 Å). *Astrophys. J.* **622**, 680–694.
- Salinas C. C. J. H., Chang L. C., Liang M.-C., Yue J., Russell J. and Mlynczak M. (2016) Impacts of SABER CO_2 -based eddy diffusion coefficients in the lower thermosphere on the ionosphere/thermosphere. *J. Geophys. Res.* **121**, 12,080–12,092. <https://doi.org/10.1002/2016JA023161>.
- Sasaki S. and Nakazawa K. (1988) Origin of isotopic fractionation of terrestrial Xe: hydrodynamic fractionation during escape of the primordial H_2 -He atmosphere. *Earth Planet. Sci. Lett.* **89**, 323–334.
- Schaefer L. and Fegley B. (2010) Chemistry of atmospheres formed during accretion of the Earth and other terrestrial planets. *Icarus* **208**, 438–448.
- Schmidt J. A., Johnson M. S. and Schinke R. (2013) Carbon dioxide photolysis from 150 to 210 nm: singlet and triplet channel dynamics, UV-spectrum, and isotope effects. *PNAS* **110**, 17691–17696.
- Chung R. W. and Nagy A. F. (1980) Ionospheres of the terrestrial planets. *Rev. Geophys. Space Phys.* **18**, 813–852.
- Sekiya M., Nakazawa K. and Hayashi C. (1980) Dissipation of the rare gases contained in the primordial Earth's atmosphere. *Earth Planet. Sci. Lett.* **50**, 197–201.
- Sekiya M., Hayashi C. and Kanazawa K. (1981) Dissipation of the primordial terrestrial atmosphere due to irradiation of the solar FUV during T-Tauri stage. *Prog. Theor. Phys.* **66**, 1301–1316.
- Shakeshaft R. and Macek J. (1972) Spin polarization in Proton-Xenon charge-exchange collisions. *Phys. Rev. A* **6**, 1876–1885.

- Sharma R. D. (2015) Technical note: on the possibly missing mechanism of 15 μm emission in the mesosphere-lower thermosphere (MLT). *Atmos. Chem. Phys.* **15**, 1661–1667.
- Sharma R. D. and Wintersteiner P. P. (1990) Role of carbon dioxide in cooling planetary thermospheres. *Geophys. Res. Lett.* **17**, 2201–2204.
- Sharp Z. D., McCubbin F. M. and Shearer C. K. (2013) A hydrogen-based oxidation mechanism relevant to planetary formation. *Earth Planet. Sci. Lett.* **380**, 88–97.
- Shelley E. G., Johnson R. G. and Sharp R. D. (1972) Satellite observations of energetic heavy ions during a geomagnetic storm. *J. Geophys. Res.* **77**(31), 6104–6110.
- Shen Y., Knudsen D. J., Burchill J. K., Howarth A. D., Yau A. W., Miles D. M., James H. G., Perry G. W. and Cogger L. (2018) Low-altitude ion heating, downflowing ions, and BBELF waves in the return current region. *J. Geophys. Res. Space Phys.* **123**, 3087–3110.
- Srinivasan B. (1976) Barites: anomalous xenon from spallation and neutron-induced reactions. *Earth Planet. Sci. Lett.* **31**, 129–141.
- Sterling N. C. and Stancil P. C. (2011) Atomic data for neutron-capture elements. III. Charge transfer rate coefficients for low-charge ions of Ge, Se, Br, Kr, Rb, and Xe^+ . *Astron. Astrophys.* **535**, A117.
- Swartz D. A. (1994) Charge transfer in helium-rich supernova plasma. *Astrophys. J.* **428**, 267–274.
- Swindle T. D. and Jones J. H. (1997) The xenon isotopic composition of the primordial martian atmosphere: contributions from solar and fission components. *J. Geophys. Res.* **102**, 1671–1678.
- Tarduno J. A., Blackman E. G. and Mamajek E. E. (2014) Detecting the oldest geodynamo and attendant shielding from the solar wind: implications for habitability. *Phys. Earth Planet. Int.* **233**, 68–87.
- Tian F., Toon O. B., Pavlov A. A. and De Sterck H. (2005) A hydrogen-rich early Earth atmosphere. *Science* **308**, 1014–1017.
- Tolstikhin I. N. and O’Nions R. K. (1994) The earth’s missing xenon: a combination of early degassing and of rare gas loss from the atmosphere. *Chem. Geol.* **115**, 1–6.
- Tolstikhin I., Marty B., Porcelli D. and Hofmann A. (2014) Evolution of volatile species in the earth’s mantle: a view from xenology. *Geochim. Cosmochim. Acta* **136**, 229–246.
- Tu L., Johnstone C. P., Güdel M. and Lammer H. (2015) The extreme ultraviolet and X-ray Sun in Time: high-energy evolutionary tracks of a solar-like star. *Astron. Astrophys.* **577**, L3.
- Urey H. C. (1952) On the early chemical history of the earth and the origin of life. *Proc. Nat. Acad. Sci.* **38**, 351–363.
- Warr O., Sherwood-Lollar B., Fellowes J., Sutcliffe C. N., McDermott J. M., Holland G., Mabry J. C. and Ballentine C. J. (2018) Tracing ancient hydrogeological fracture network age and compartmentalisation using noble gases. *Geochim. Cosmochim. Acta* **222**, 340–362. <https://doi.org/10.1016/j.gca.2017.10.022>.
- Watson A., Donahue T. M. and Walker J. C. G. (1981) The dynamics of a rapidly escaping atmosphere: applications to the evolution of Earth and Venus. *Icarus* **48**, 150–166.
- Weiss B. P., Fu R. R., Einsle J. F., Glenn D. R., Kehayias P., Bell E. A., Gelb J., Araujo J. F. D. F., Lima E. A., Borlina C. S., Boehnke P., Johnstone D. N., Harrison T. M., Harrison R. J. and Walsworth R. L. (2018) Secondary magnetic inclusions in detrital zircons from the Jack Hills, Western Australia, and implications for the origin of the geodynamo. *Geology* **46**, 427–430.
- Wordsworth R. and Pierrehumbert R. T. (2013) Hydrogen-nitrogen greenhouse warming in Earth’s early atmosphere. *Science* **339**, 64–67.
- Yelle R. V. (2004) Aeronomy of extra-solar giant planets at small orbital distances. *Icarus* **170**, 167–179.
- Zahnle K. J. and Walker J. C. G. (1982) Evolution of solar ultraviolet luminosity. *Rev. Geophys. Space Phys.* **20**, 280–292.
- Zahnle K. J. and Kasting J. F. (1986) Mass fractionation during transonic escape and implications for loss of water from Mars and Venus. *Icarus* **68**, 462–480.
- Zahnle K. J., Kasting J. F. and Pollack J. B. (1990) Mass fractionation of noble gases in diffusion-limited hydrodynamic hydrogen escape. *Icarus* **84**, 502–527.
- Zahnle K. J., Claire M. W. and Catling D. C. (2006) The loss of mass-independent fractionation in sulfur due to a Paleoproterozoic collapse of atmospheric methane. *Geobiology* **4**, 271–283.
- Zahnle K. J., Schaefer L. and Fegley B. (2010) Earth’s Earliest Atmospheres. In *The Origin of Cellular Life* (eds. D. Deamer and J. W. Szostak), pp. p 49–65. Cold Spring Harbor Perspectives in Biology. Cold Spring Harbor Laboratory Press, NY.
- Zahnle K. J., Catling D. C. and Claire M. W. (2013) The rise of oxygen and the hydrogen hourglass. *Chem. Geol.* **362**, 26–34.
- Zerle A. L., Claire M. W., Domagal-Goldman D., Farquhar J. and Poulton S. W. (2012) A bistable organic-rich atmosphere on the Neoproterozoic Earth. *Nature Geosci.* **5**, 359–363.

Associate editor: Nicholas Dauphas